 doi:10.20944/preprints201702.0029.v1

Article

Neutral Low-Dimensional Assemblies of a Mn(III) Schiff Base Complex and Octacyanotungstate(V): Synthesis, Characterization and Magnetic Properties

Anna M. Majcher,[2] Guillaume Pilet,[3] Vladimir S. Mironov[4] and Kira E. Vostrikova*[1]

[1] Nikolaev Institute of Inorganic Chemistry SB RAS, Lavrentiev avenue 3, Novosibirsk 630090, Russia; vosk@niic.nsc.ru
[2] [2]Institute of Physics, Jagiellonian University,Lojasiewicza 11, PL-30348 Krakow, Poland; anna.majcher@uj.edu.pl
[3] Laboratoire des Multimatériaux et Interfaces (UMR 5615), Université Claude Bernard Lyon 1, 69622 Villeurbanne Cedex, France; guillaume.pilet@univ-lyon1.fr
[4] Shubnikov Institute of Crystallography of Federal Scientific Research Centre "Crystallography and Photonics" RAS, Leninsky prospect 59, 119333 Moscow, Russia; mirsa@list.ru

* Correspondence: vosk@niic.nsc.ru

Abstract: Two novel low-dimensional molecular magnetic materials were prepared by a self-assembling of 3d- and 5d-metal complexes. These are the first neutral heterobimetallic cyanobridged compounds involving one anisotropic Mn(III) Schiff base complex and one octacyanotungstate(V) per molecular unit. A slow diffusion of the constituents' solutions leads to a formation of the 0D crystalline complex **1** due to coordination of a water molecule to the Mn center prevents a polymer formation. A rapid mixing of reagents results in a precipitation of the microcrystalline powder of the complex **2**, which on a totality of experimental data possess 1D polymeric structure. The magnetic studies have shown that antiferromagnetic exchange interactions are dominating in **1** J/k_B= -13.1(7) K, D=-3.0(1.3) K, zJ'= -0.16(20) K and g_{av}=2.00(1); while the presence of the significant intramolecular Mn(III)–W(V) ferromagnetic couplings through cyanide bridges is characteristic for **2** (J/k_B = 46.1(5) K g_{Mn} = 2.11(3), fixed g_W = 2.0). Due to the weak interchain interactions, zJ'/k_B = –0.8(2) K, compound **2** is a metamagnet with the Néel temperature of 9.5 K undergoing a spin-flip transition at 2 kOe. The slow magnetization dynamics of **2** was investigated at DC field of 0 and 2 kOe, giving the values of τ_0 32(15) and 36(15) ps respectively, well within the range typical for SCMs. The respective Δ_τ/k_B values were 48.4(1.2) and 44.9(1.0) K.

Keywords: cyanide-bridged heterometallic assemblies; octacyanotungstate(V); Mn(III) Schiff base complexes; single-chain magnet; 1D coordination polymers; metamagnet; ferromagnetic coupling

1. Introduction

Molecular magnets of low dimensionality representing polynuclear coordination compounds in which the paramagnetic ions linked together via bridging ligands are particularly interesting due to slow magnetic relaxations a large group among them exhibit. What makes them especially attractive is the fact that they are very likely to find applications in *e.g.* high-density data storage or quantum computers [1-4]. A key parameter to describe these materials is the anisotropy energy barrier, Δ_A, which needs to be overcome to reverse the magnetization.

For the zero-dimensional (0D) systems named single-molecule magnets (SMMs) the Δ_A value depends on the total spin and the energy of uniaxial anisotropy the molecule and can be expressed as $\Delta_A = S^2|D|$ for integer S and $(S^2 - 1/4)|D|$ for half-integer S [4], where the axial zero-field splitting parameter, $D < 0$. In order to use SMM in real devices or at least in their prototypes the Δ_A should be

Preprints (www.preprints.org) | NOT PEER-REVIEWED | Posted: 9 February 2017 doi:10.20944/preprints201702.0029.v1

high enough to fix the magnetic moment orientation and to prevent quantum tunneling. Slow magnetic relaxation has also been found for one-dimensional (1D) coordination compounds, known as single-chain magnets (SCMs) [5-27]. In terms of greater relaxation barrier, SCMs possess an advantage over SMMs. This benefit originates from an additional contribution in Δ_A, yclept correlation energy Δ_ξ, which provided by the exchange coupling (J) between the paramagnetic centers. Taking into account that an interaction between adjacent spin carriers is $-2JS_1 \cdot S_2$, $\Delta_\xi = 4|J|S^2$, for an isotropic model when $|D/J| > 4/3$ (Ising limit), while when $|D| << |J|$, $\Delta_\xi = 4S^2|JD|^{1/2}$ (Heisenberg limit) [2,7]. Therefore, for an infinite magnetic chain the total spin reversal barrier can be written as $U_{eff} = \Delta_A + 2\Delta_\xi$ [28-30]. However, in a finite-length spin chain the contribution of the correlation energy to the U_{eff} is twice smaller ($U_{eff} = \Delta_A + \Delta_\xi$) due to a nucleation effect of the chain ends. Indeed, at low temperatures the relaxation dynamics of SCMs is typically described by the finite-length model [11].

Cyano-bridged metal assemblies have provided a large number of compounds with SMM [31-38] and SCM behavior [39-48]. The greater part of these materials comprises 3d metal ions as the core magnetic units. This can be explained by the fact that compared to their 4d and 5d congeners the coordination chemistry of the first row transition metals complexes is well studied, and there are numerous theoretical models to describe their magnetic behavior. The use of heavier transition metal complexes in the design of low-dimensional nanomagnets has a better hand. First of all they possess more diffuse valence orbitals than 3d metals that can provide stronger magnetic exchange interactions [32]. Further, the ions of these metals can be in different oxidation states having a small difference in the ox-red potentials that is favorable to generate charge transfer reactions by electrical or light irradiation. The latter phenomenon is useful for the preparation of multifunctional materials possessing such property as photomagnetism [49-51].

Compounds involving cyanide complexes as metalloligands are the most common in the area of 4d and 5d molecular magnetism [32], the majority of cyanobridged heterometallic assemblies including the octacyanometallates [50-52]. Some of them are 1D polymers [53-56]; others possess layered [57-63] or 3D network structure [64-68]. The paramagnetic cyanotungstate(V) tectones have been used to build discrete molecules [69-71], chains [53-56], 2D [57] and 3D networks [64-68] and some of them have displayed variable magnetic properties such as high ordering temperatures [72], photo-induced magnetism [73,74], SMMs [75], and SCMs [17,54,55]. However, the assemblies of the paramagnetic $[W(CN)_8]^{3-}$ precursor and manganese(III) Schiff base complex, $[Mn(SB)]^+$, are fairly limited and poorly studied in comparison with the large family of bimetallic compounds comprising of $[Mn(SB)]^+$ cation and the 3d metal hexacyanides that are extensively investigated both structurally and magnetically [76]. To the best of our knowledge, so far only six bimetallic low-dimensional magnetic systems involving $[Mn(SB)]^+$ and $[W(CN)_8]^{3-}$ units have been reported [55,54,69-71,77].

To compensate the triple charge of the $[W^V(CN)_8]^{3-}$ unit three $[Mn(SB)]^+$ moieties are needed. Thus, the nuclearity of molecular {MnW} species varies depending on a structure of SB-ligand. In comparison with *acacen*$^{2-}$ (N,N-ethylenebis(acetylacetonylideneiminato)) included in the layered complex $K[Mn(acacen)]_2[W(CN)_8]\cdot 2H_2O$ [57], the *salen*-type ligands are too large to be assembled through the three cyano bridges in tetranuclear neutral moiety $[Mn(SB)]_3[W(CN)_8]$. Even in the case of the smallest di-anion ligand *salen*$^{2-}$ (N,N′-ethylenebis(salicylideneiminato)) only two Mn^{III}-centers in $[Mn(salen)H_2O]_3[W(CN)_8]$ [70] are bound directly to the cyanometallate unit and the third one is phenolate-bridged to {W-CN-Mn(salen)} unit forming an Mn–NC–W–CN–Mn–O_{PheO}–Mn skeleton. Two closely related tri-nuclear compounds: $[Mn(^{5Cl}salmen)(H_2O)_2]\{[Mn(^{5Cl}salmen)H_2O]_2W(CN)_8]\}$ (^{5Cl}salmen^{2-}=N,N′-(1-methyl-ethylenebis(5-chlorosalicylideneiminato)) [77] and $[Mn(^{5Cl}saltmen)H_2O(MeOH)]\{[Mn(^{5Cl}saltmen)H_2O][Mn(^{5Cl}saltmen)MeOH]W(CN)_8\}$ (^{5Cl}saltmen^{2-}=N,N′-(1,1,2,2-tetramethylethylene)bis(5-chlorosalicylidene-iminato)) [71] have a separated $[Mn(^{5Cl}SB)(Solv)^2]^+$ cation, while in the binuclear complex $[Mn(^{3MeO}salophen)(H_2O)_2]_2\{[Mn(^{3MeO}salophen)H_2O][W(CN)_8]\}$ (^{3MeO}salophen^{2-} = N,N′-phenylenebis(3-methoxysalicylideneiminato)) [69] the hydrogen bonds between aqua ligands as well as π–π contacts between aromatic rings bound the neighboring $\{Mn^{III}W^V\}^2$-dimer and isolated Mn^{III} moiety. Both known to date SCMs, involving $[W^V(CN)_8]^{3-}$: $[Mn(^{5Br}salen)(H_2O)_2]\{[Mn(^{5Br}salen)H_2O][Mn(^{5Br}salen)W(CN)_8]\}$ (^{5Br}salen^{2-} = N,N′-ethylenebis(5-bromo-salicylideneiminato)) and $[Mn(L)(H_2O)_2]_2[Mn(L)W(CN)_8]$, H_2L = N,N′-bis(2-hydroxynaphthalene-1-carbaldehydene)-1,3-diaminopropane) [55] also comprise separated $[Mn(SB)(H_2O)_2]^+$ counter ion, dimerized or not.

Preprints (www.preprints.org) | NOT PEER-REVIEWED | Posted: 9 February 2017 doi:10.20944/preprints201702.0029.v1

For a large variety of the self-assembling in {[Mn(SB)H_2O]$^+$–[W(CN)$_8$]$^{3-}$} system the rational design of the low-D magnetic materials is not possible due to a random localization of both bridged and separated paramagnetic anisotropic units of [Mn^{III}(SB)(H_2O)$_2$]$^+$ in the crystals of heterobimetallic complexes. The main approach for the telic synthesis of 0-1D species is a preparation of the neutral $Mn^{III}W^V$ magnetic assemblies. To implement this objective, once charged heteroligand cyanide species [WL(CN)$_6$]$^-$ (L = bipyridine or phenantroline) have been used [78-81]. Despite the successful synthesis of the few [Mn(SB)][WL(CN)$_6$] compounds with SCM behavior, this way has an essential drawback because the yield of octacoordinated [WL(CN)$_6$]$^-$ precursors is low [80]. Very recently, the neutral molecular dimeric complexes were studied [82], as well as a row of chain coordination polymers [48] comprised of 3d metals cyanides, [M^{III}(CN)$_6$]$^{3-}$, and triply charged [Mn^{III}(SB^{2+})]$^{3+}$-unit presented in Scheme 1. This choice was driven by the following factors: i) Mn^{III} unit with a total "3+" charge can provide an assembling of neutral {Mn^{III}SB}/{M^{III}(CN)$_6$} 1:1 complexes due to electrostatic attraction; ii) besides, the large $(CH_3)_3N^+$ groups of the 5TMAMsalen ligand should contribute to an axial coordination of the [Mn(5TMAMsalen)]$^{3+}$ cations to the [M^{III}(CN)$_6$]$^{3-}$ anion upon and iii) to separate spatially the final 1D-polymers to cancel or reduce interchain magnetic interactions through the joint impact of both charge repulsion and sterical hindrance [48].

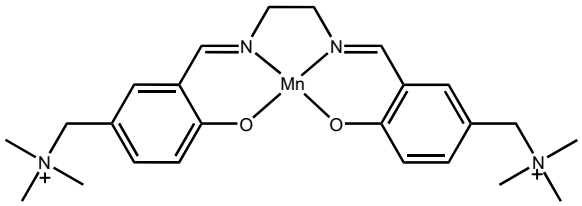

Scheme 1. Triply charged unit [Mn^{III}(SB^{2+})]$^{3+}$.

In the present report we have extended this tactic onto the synthesis of a dinuclear complex [Mn^{III}(5TMAMsalen)(H_2O)W^V(CN)$_8$](H_2O)$_{4.75}CH_3CN$ (**1**) and a coordination chain polymer [Mn^{III}(5TMAMsalen)W^V(CN)$_8$](H_2O)$_8CH_3CN$ (**2**) composed of equally charged constituents. The compounds were characterized by IR, TG, XRD and elemental analysis. The detailed magnetic measurements were performed for both complexes. An explicit analysis of the magnetic properties together with a set of the other studies has revealed that **2** is a metamagnetic chain compound exhibiting slow relaxation of magnetization.

2. Results and Discussion

2.1. Preparation and Characterization

It is very important to underline that both compounds were synthesized using a stoichiometric 1:1 molar ratio of the constituents by reactions of acetonitrile solution of [Mn(5TMAMsalen)(H_2O)$_2$](ClO_4)$_3$(H_2O) with aqueous K_3[W(CN)$_8$](H_2O)$_2$. A diffusion method was implied for **1**, while a direct mixing of the precursors solutions, followed by heating, for 2. The latter can also be obtained starting from **1** (See experimental section). The diffusion route gives **1** in the form of long brown-yellowish parallelepiped-like batons in a high yield, while a precipitation route results in a dark brown-reddish powder with quantitative yield. Doubtless, that the inter-diffusion of aqueous and acetonitrile solutions produces the binuclear complex due to the coordination of an aqua-ligand to the Mn end of the {W-Mn} unit. Therefore, to avoid this process it's necessary to use the non-coordinating solvents along with the assembling of the chain polymer [Mn(SB)W(CN)$_8$]$_n$. However, all our attempts to grow the single crystals of 1D material using dry nitromethane and dichloromethane (or chloroform) as solvents for Mn- and W-precursors respectively were failed. If in the case of layering, for all solvent combinations, on the interface between two solutions an impenetrable membrane preventing further contacts of the components was formed, then a direct mixing has resulted in amorphous powders. Very often, these powders were contaminated by product containing perchlorate anion, registered by IR.

Preprints (www.preprints.org) | NOT PEER-REVIEWED | Posted: 9 February 2017 doi:10.20944/preprints201702.0029.v1

Table 1. ν(CN) frequencies for **1**, **2** and $(Bu_4N)_3[W(CN)_8]$ (cm^{-1}).

1	$(Bu_4N)_3[W(CN)_8]$ [83]	**2**
2165.7sh		2167.6sh
2161.8		2161.8
2138.7	2141	2146.4
2127.1	2130	2129.0sh
2121.3	2123	
2100.0		2111.7
2084.0		2088.0
2033.0		2038.4

At room temperature during a period of few weeks the crystals of **1**, being enclose in a vial, lose partially the solvated water keeping their crystallinity without deterioration of the X-ray diffraction quality. **1** and **2** are gradually losing the solvent molecules during storage and heating. A thermo-analytical investigation of **1** has shown, that in the temperature range of 25 – 145 ºC the solvent loss of ~ 13.5 % (12.87 % calculated for $[Mn(5TMAMsalen)(H_2O)][W(CN)_8](H_2O)_{4.75}(CH_3CN)$) occurs in two steps. The first one (~11.5 %) most likely corresponds to the evaporation of four non-coordinated solvent: four water molecules and one CH_3CN molecule, while the second step (~2%) is caused by a release of the coordinated H_2O (See Figure S1 of Supplementary information (SI)).

The powder samples of **2**, depending on their dispersity, lose the solvent molecules with a different speed. For this reason a solvent content in **2** was determined by heating of a part of freshly prepared sample under vacuum at 110 ºC up to constant sample weight wherein the weight loss was 17%. A treated in such manner sample as well as its progenitor was analyzed for CHN content. The heated in mild conditions powders of **2** absorb some amount of water from air, that is confirmed by a weight loss step on a TG curve (See Figure S1, SI). An intensive decomposing of the complexes starts above 200 ºC. It is necessary to emphasize that **2** is somewhat thermally stable compared to **1**, which is clearly visible in the Figures S1 and S2, where TG and DTG plots for both complexes are presented. Highest thermal stability of **2** is consistent with the polymeric structure.

The compounds have very similar IR spectra in the range 1700–400 cm^{-1}, where the majority of frequencies matches the coordinated Schiff base ligand frequencies. The broad absorptions are centred at 3440 and 3417 cm^{-1} for **1** and **2** respectively, being more intensive for the latter. Such a broad peak indicates existence of a system of hydrogen bonds. In the region 2100÷2030 cm^{-1} both complexes have a complicated rake of peaks characteristic for CN vibration stretches (See Table 1). The presence of a set of bands indicates that the cyanide groups in $[W(CN)_8]^{3-}$ are partly included in different type of interactions (bridging, hydrogen bounding). Note that for **2** the majority of ν_{CN} peaks is slightly shifted towards higher frequencies compared to those of **1**. This may be associated with a more linked character of $[W(CN)_8]^{3-}$ metalloligand, which evidences in favor of polymeric nature of **2**.

2.2. Description of Molecular Structure

Crystallographic data and structure refinement summary for **1** is included in Table 2. Single crystal X-ray structural analysis has demonstrated that this compound has a 0D molecular structure with an asymmetric unit (Figure 1) representing a neutral bimetallic assembly and consisting of one $[W(CN)_8]^{3-}$ anion and one $[Mn(5TMAMsalen)(H_2O)]^{+}$ cation. The slightly distorted square antiprism coordination environment of tungsten ion comprises eight cyanide ligands. Some bond distances and angles defining the coordination polyhedrons geometry are shown in Table 2. The W–C bond distances vary from 2.151(7) to 2.168(6) Å with average value of 2.156(6) Å and W–C–N angles are close to 180 º with a greatest deviation from linearity of 1.58 º, which is consistent with the data obtained for related compounds [50,57,69,70,77]. The coordination environment of the Mn ion is an elongated tetragonal bipyramid because of the Jahn-Teller distortion. The 2O and 2N donor atoms of the 5TMAMsalen ligand in the basal plane of the pyramid form shorter bonds of 1.873–1.989 Å, while one N atom and an O atom of H_2O molecule in axial positions form much longer (2.244–2.447

Preprints (www.preprints.org) | NOT PEER-REVIEWED | Posted: 9 February 2017 doi:10.20944/preprints201702.0029.v1

Å) (Table 2). The Mn–N–C bond angle is less than 180° and equal to 160.8°. Such a flexion is typical for the cyanide bridged Mn^{III}–$M(CN)_n$ complexes [69-71,57,77,82,84,85].

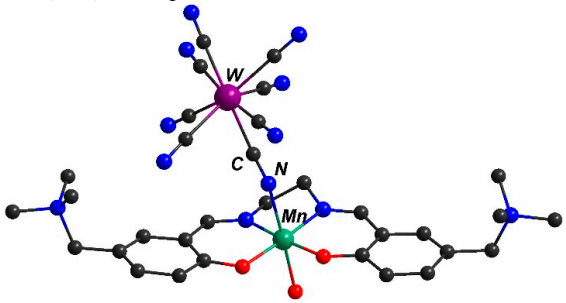

Figure 1. Molecular structure of the [Mn(5TMAMsalen)(H_2O)W$(CN)_8$] unit in 1. Hydrogen atoms are omitted for clarity.

Table 2. Selected bond distances (Å) and angles (º) for **1**.

[Mn(5TMAMsalmen)]$^{3+}$moiety	
Mn–$O_{phenolate}$	1.873(4)
	1.895(3)
Mn–N_{imine}	1.985(4)
	1.989(4)
Mn–O_{water}	2.247(4)
Mn–$N_{cyanide}$	2.244(4)
Mn–N≡C	160.8(3)
N_{imine}–C–C–N_{imine}	43.3(6)
$[W(CN)_8]^{3-}$ moiety	
M–$C_{cyanide}$	2.154(6)
	2.152(5)
	2.159(5)
	2.157(6)
	2.168(6)
	2.152(5)
	2.153(6)
	2.151(7)

As in the case of related 0D [82] and 1D [48] compounds, $[Mn^{III}(SB^{+})M^{III}(CN)_6(H_2O)]$, M^{III} = Fe, Mn, and Cr, the Schiff-base ligand is in an *envelope* conformation with a torsion angle comprising the N_{imine}–C–C–N_{imine} core and a dihedral angle between aromatic rings. In addition, unlike the reported in ref. 48 SCMs in **1** the positively charged triethylammonium groups are in a cis-position relatively the $[Mn^{III}$(5-TMAMsalen)$]^{3+}$ complex similarly to its 3d-congener described in ref. 82.

The neutral bimetallic units of [Mn(5TMAMsalen)(H_2O)W$(CN)_8$] are bound into pairs by the hydrogen bonds between aqua ligands and phenolate oxygen as well as π–π contacts of 3.34 Å between aromatic rings (Figure 2). The distance of 4.906 Å between adjacent Mn ions is shorter than that of 5.278 Å found in [Mn($^{5\text{-}Cl}$saltmen)H_2O(MeOH)]{[Mn(^{5Cl}saltmen)(H_2O)Mn(^{5Cl}saltmen)(MeOH) W$(CN)_8$]} [71]. Four from the seven non-bridging cyanide groups of the $[W(CN)_8]^{3-}$ anion are included in intermolecular 3D hydrogen-bonding network, see Figure 2. In the crystal lattice there are seven positions occupied by H_2O molecules with the total occupancy of 3.75 and one MeCN molecule, which is not included in hydrogen bonding.

The powder XRD data for **2** are presented in Figure S3, SI. The diffractogram of **2** differs from PXRD simulation of **1** and related chain compound {[Mn(5TMAMsalen)][Fe$(CN)_6$]}$_n$ [48]. Considering the fact that the compound **2** have the composition of [Mn(5TMAMsalen)W$(CN)_8$] (H_2O)$_8$(CH_3CN) with 1: 1 ration for Mn:W, two organization of a bimetallic product in the solid are possible. One of them is a tetranuclear moiety formed from the two dimers [Mn(5TMAMsalen)(H_2O) W$(CN)_8$] by removing the aqua ligands coordinated to Mn-centers. This can result in a new 1D

Preprints (www.preprints.org) | NOT PEER-REVIEWED | Posted: 9 February 2017 doi:10.20944/preprints201702.0029.v1

assembly by means of a mutual bridging of the {Mn(5TMAMsalen)} units by phenolate oxygen atoms similar to in ref [47] and forming the $_7$(CN)-W-CN-Mn(-O-)$_2$-Mn-NC-W(CN)$_7$ core. However, in such a case the valence stretches of CN would not experience some significant shifting in higher frequencies as it take place for **2**. Another option at the 1:1 metal ratio is a coordination linear polymer comprising of the –CN–Mn–NC–W– repeating moieties. This molecular structure of the compound is in better agreement with the experimental data.

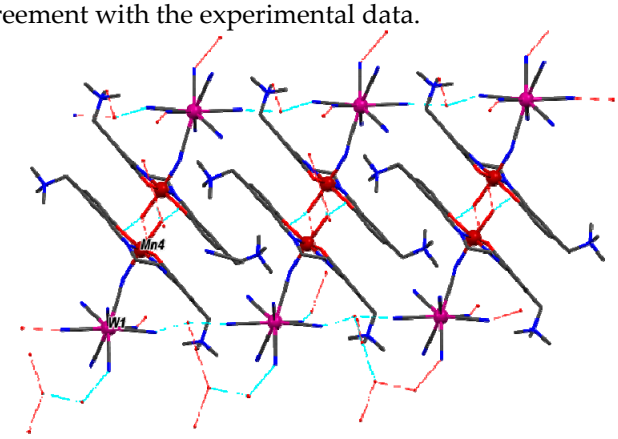

Figure 2. System of hydrogen bounding in **1**. Hydrogen atoms are omitted for clarity.

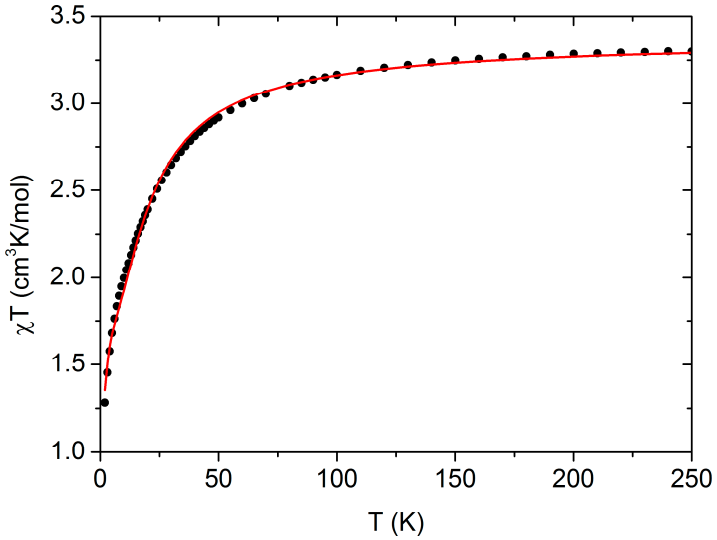

Figure 3. The temperature dependence of the χT product for **1**. The solid line represents the fitted χT values (see text).

2.3. Magnetic properties

2.3.1. Magnetic behavior of **1.**

The temperature dependence of the χT product for 1 is presented in Figure 3. The χT value at 250 K is 3.30 cm^{3}K/mol, which is very close to 3.34 cm^{3}K/mol expected for the high temperature limit for a pair of spins S_{Mn} = 2, S_W = 1/2 and g = 2. χT decreases monotonically, pointing to an antiferromagnetic interaction between the spins, and reaches ~ 1.3 cm^{3}K/mol at 2 K that is smaller than 1.87 cm^{3}K/mol expected for the total spin 3/2 in the ground state of antiferromagnetically coupled Mn^{III} and W^{V}. This may be associated with the zero-field splitting in Jahn-Teller distorted Mn^{III} complex, or/and antiferromagnetic intermolecular interaction. No sign of magnetic ordering was observed down to 1.8 K, using low field ZFC/FC and AC susceptibility measurements (See Figures S4 and S5 in SI).

To simulate the magnetic behavior of **1** we used the model of two spins with a Heisenberg exchange interaction J between them. The zero-field splitting of Mn^{III} was taken into account using the axial approximation with D term only.

Preprints (www.preprints.org) | NOT PEER-REVIEWED | Posted: 9 February 2017 doi:10.20944/preprints201702.0029.v1

$$\hat{H} = -JS_{Mn}S_W + D\left[S_{z,Mn}^2 - S_{Mn}(S_{Mn}+1)\right] - g\mu_B(\mathbf{S}_{Mn}+\mathbf{S}_W)\cdot\mathbf{H} \qquad (1)$$

The Hamiltonian (1) was diagonalized numerically to calculate the magnetization of isolated Mn-W pairs $M_2(H,T)$. The value averaged over **H** directions was calculated to account for the powder sample. The inter-dimer interaction was introduced in the mean-field model numerically solving the equation for magnetization $M(H,T) = M_2(H + \lambda M, T)$, where $\lambda = zJ'/N_A\mu_B^2g^2$. The least square fit of the temperature dependence of susceptibility (Figure 3) has resulted in the following parameters: J = -13.1(7) K, D = -3.0(1.3) K, zJ' = -0.16(20) K and the average factor g = 2.00(1). The values of D and zJ' are strongly correlated, which leads to their significant uncertainty.

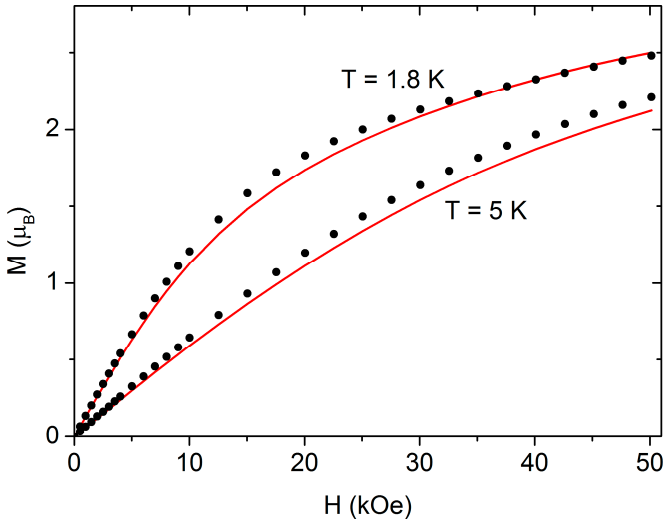

Figure 4. Magnetization of **1** versus magnetic field measured at 1.8 and 5 K. Solid lines are calculated M(H) dependencies (see text).

Based on the values of ZFS for Mn^{III} in a similar environment [82] the negative sign of D was assumed for the initial parameters in the fitting procedure. A value of D obtained from the susceptibility fit was used to calculate $M(H)$ dependencies shown in Figure 4. At zJ' = 0, the obtained parameters were D = -3.8(2) K, J = -13.6(2) K, and g = 2.00(1) with almost the same fit quality judged by R^2 value. The values of these fitting parameters are closed to those found for a related anionic chain $[Zn(HC(3,5\text{-}Me_2pz)_3]_2[W(CN)_8Mn(^{5\text{-}Br}salcy)]$ [56].

In order to verify the consistence of the mean-field term zJ' value, it is important to evaluate the strength of spin coupling between two Mn^{III} ions involved in two neighboring $[Mn^{III}(5TMAMsalen)(H_2O)$ units, which is mediated by hydrogen bonds between water ligands and π–π contacts between aromatic rings of the closest $[Mn^{III}(SB^+)]$ (See Figure S6, SI). For this purpose we have calculated the $J_{Mn\text{-}Mn}$ exchange parameter in the $[(MnSB^+(H_2O)]_2$ moiety (Figure S6, SI) in terms of a microscopic model based on the multi-electron superexchange theory described in ref [86]; details of such calculations are reported in [87-89].

Electronic characteristics of a pair of Mn^{III} ions were obtained from ligand-field (LF) calculations in combination with the angular-overlap model (AOM) [90]. In these calculations, the AOM parameters e_σ(O,N)=10000 cm^{-1} and e_σ(O,N)/e_π(O,N)=0.25 were employed (at the average metal-ligand distance of R_0(Mn–O)=2.05 Å), the radial dependence of the AOM parameters having been approximated by $e_{\sigma,\pi}(R)=e_{\sigma,\pi}(R_0)\ (R_0/R)^n$ with n=4. LF calculations for Mn^{III} ions in the $\{MnSB^+(H_2O)\}$ unit were performed with the B = 600 and C = 3400 cm^{-1} Racah parameters and The Mn→Mn charge-transfer energy fixed at $U_0(W \rightarrow Mn)$=65000 cm^{-1} (8 eV). The set of one electron matrix elements, $\langle d_i(A)|h|d_j(B)\rangle$, related to magnetic orbitals $3d_i(A)$ and $3d_j(B)$ (with the orbital indexes i, j = xy, yz, zx, $x^2–y^2$, and z^2) and centered on the pair of Mn^{III} ions was obtained from extended Hückel calculations based on the atomic parameterization reported in [91] as well as a real geometry of the $\{(MnSB^+(H_2O)\}_2$ unit (Figure S6, SI) using the projection procedure described in [92].

Our calculations have resulted in a small antiferromagnetic exchange parameter $J_{Mn\text{-}Mn}$ of –0.033 cm^{-1} (–0.048 K), which is much smaller than the exchange parameter $J_{Mn\text{-}W}$ of –13.6 K within the

Preprints (www.preprints.org) | NOT PEER-REVIEWED | Posted: 9 February 2017 doi:10.20944/preprints201702.0029.v1

dimer. This provides an evidence that hydrogen bonds along with the π–π contacts between ligand aromatic rings are poor mediators of spin coupling between Mn^{III} ions in the $\{(MnSB^{+}(H_2O)\}_2$ unit. This suggests that {[Mn(SB⁺)H₂O] [W(CN)₈]} molecular clusters are magnetically isolated and do not form 1D magnetic chains in the structure of **1**. It is also noteworthy that the calculated parameter $J_{Mn\text{-}Mn}$ of –0.048 K is reasonably consistent with the value of the molecular field parameter zJ' = -0.16(20) K obtained from the fitting calculations. This justifies the use of the approach of isolated W-Mn dimers in terms of eq. (1).

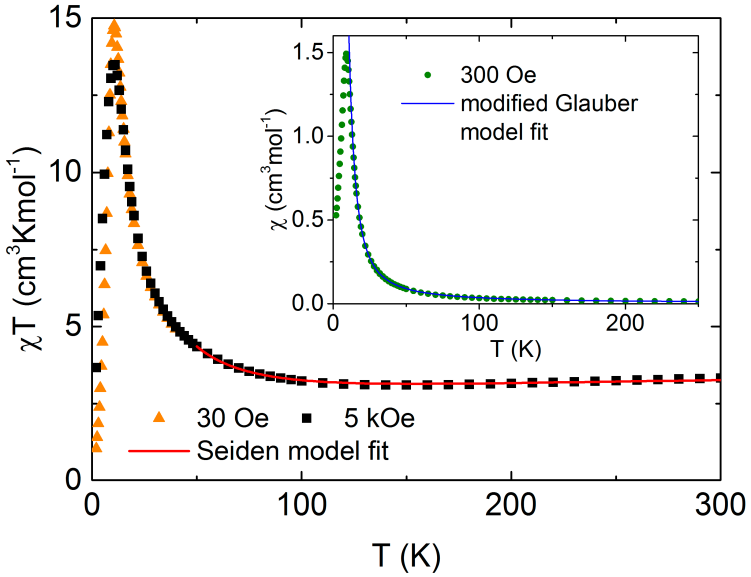

Figure 5. The temperature dependence of the χT products for 2 at different fields. Red solid line represents a Seiden model fit to the 5 kOe data. Inset: χ as a function of temperature in 300 Oe with a modified Glauber model fit (See in the text).

2.3.1. Magnetic behavior of **2.**

The cryomagnetic data for **2** is noticeably different from those for **1**. The temperature dependences of the χT product for **2** obtained at magnetic field of 30 Oe and 5 kOe are presented in Figure 5. Starting from a constant value of 3.3 cm^3Kmol^{-1} at high temperatures, χT values begin to rise reaching a peak of 10.4 and 10.7 cm^3Kmol^{-1} at 15 K for data obtained at 5000 and 30 Oe, respectively, before dropping sharply at lower temperatures for both. Such a behavior was also observed in [Mn(SB)]₂[Mn(SB)W(CN)₈] [54,56], K[Mn(acacen)]₂[W(CN)₈]·2H₂O [57], and indicates the presence of significant intramolecular Mn^{III}–W^{V} ferromagnetic interactions through cyanide bridges. A fit of the Seiden model [93] of an alternating chain composed of Heisenberg spins ½ and 2 described by the Hamiltonian (2)

$$\hat{H} = -J\sum_i (S^i_{Mn} + S^{i+1}_{Mn}) \cdot S^i_W \quad (2)$$

to the data obtained at 5 kOe in the temperature range 50-300 K was performed using a single coupling constant J value, assumed identical for all W-Mn pairs, and $g_W = 2.0$ fixed. This approximation has delivered $g_{Mn} = 2.11(3)$ and $J = 46.1(5.2)$ K, which indicates enough strong ferromagnetic coupling between W and Mn centers similar to data of Hong's group [54].

Additionally, to estimate the interactions between the chains, the classic Glauber model $\chi T = C_{eff}\exp(\Delta\xi/T)$ [28] was modified by including the following equation from the mean field theory [94] that accounts for the interaction between the chains: $\chi = \chi_{chain}(1\text{-}zJ'/(2N_A g^2 \mu_B^2)\chi_{chain})$, where χ represents the susceptibility of a system with weakly interacting chains, χ_{chain} is the susceptibility of isolated chains, and zJ' is a measure of the interchain interaction. The parameters obtained from the fit of the aforementioned model to the data obtained in 300 Oe in the temperature range 15-50 K are as follows: the domain wall formation energy $\Delta\xi/k_B = 22.5(5)$K, $C_{eff} = 2.91(4)cm^3Kmol^{-1}$ and $zJ'/k_B = -0.8(2)$ K (–0.53(9)cm^{-1}) (assuming effective $g = 2.0$), which is within the range for metamagnetic SCMs [95,96].

Preprints (www.preprints.org) | NOT PEER-REVIEWED | Posted: 9 February 2017 doi:10.20944/preprints201702.0029.v1

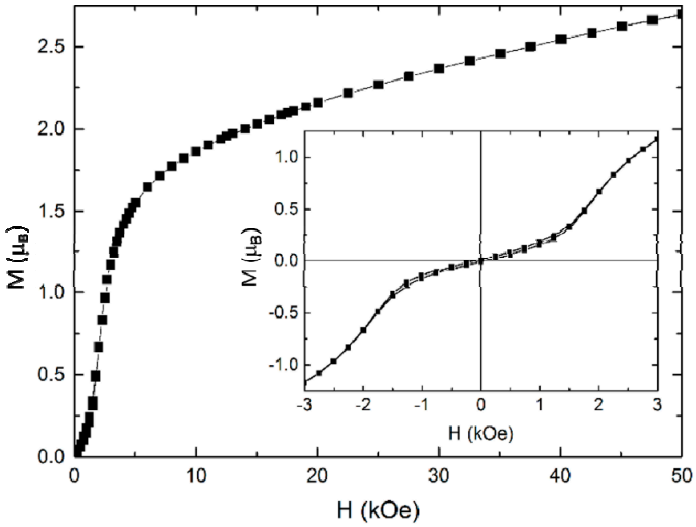

Figure 6. The magnetization of **2** versus field in T = 2 K. Inset: magnified low-field region. The solid lines are to guide the eye.

The magnetization vs. field curve of **2** measured at 2 K (Figure 6) proves that the compound is a metamagnet which undergoes a spin-flip transition at 2 kOe. The M value reached at 50 kOe is equal to 2.7 μ_B per Mn^{II}-W^{V} unit, which is far from the theoretical value of 5.0 μ_B expected for ferromagnetically coupled Mn^{III} ion with S=2 and W^{V} with S=1/2 and g_{av} = 2.0. The estimated saturation magnetic field, H_A, for **2** is about 91 kOe, of the same order the values of 100, 108 and 120 kOe found for SCMs based on neutral [Mn(5TMAMsalen)(Cr/Fe)(CN)$_6$] [48] and anionic $[Mn^{III}(acacen)Fe^{III}(CN)_6]^{2-}$ [85] fragments respectively. It is a consequence of the Mn^{III} ion anisotropy. The antiferromagnetic behavior at low fields is further confirmed by the zero-field cooling/field cooling experiment (Figures S6 and S7, SI), from which the Néel temperature of 9.5 K is clearly visible. Our previous analysis of the thermal dependence of the χT product explains this metamagnetic behavior, which is derived from weak antiferromagnetic interactions between ferromagnetically coupled chains.

The AC susceptibility of **2** reveals frequency dependence below 4 K (Figures S8, S9, SI). Considering the metamagnetic character of this compound, measurements of AC susceptibility versus applied DC field were performed at four different temperatures (Figure S9, SI). They show significant maxima for H_{DC}=2 kOe which concurs with the value of the spin-flip field. As slow magnetic relaxations in such systems can be enhanced by applying sufficient DC field [30], AC measurements were conducted with DC field of 2 kOe applied as well. In these conditions, the frequency dependence became more visible, which is shown in Figures S8 and S10 (SI). The Mydosh parameter, defined as the temperature shift of the χ' peak on a decade of frequency $\Delta T_m/[T_m\Delta\log(\upsilon)]$, equals 0.13, which is above the range typical for spin-glasses [97].

Due to the DC field dependence, frequency plots of the AC susceptibility for **2** were measured at H_{DC} = 0 and 2 kOe over a series of temperatures (Figure S10, SI). Generalized Debye model [98] was fitted to χ' and χ'' simultaneously for each temperature. The fitted parameters were χ in the limits χ_0 and χ_∞, the relaxation time τ and the parameter α describing the distribution of τ. The fits for **2** delivered the α values in the range 0.12-0.38 and thus confirmed the SCM character of the assembly. The parameters τ and α are listed in Table S1, SI.

Plots of ln(τ) versus T^{-1} for **2** derived from the generalized Debye model fits to the data in 0 and 2 kOe DC fields are presented in Figure 7. The values obtained from linear fits of the Arrhenius law $\ln\tau = \ln\tau_0 + \Delta_\tau/(k_BT)$ of τ_0 were similar and equal 32(15) and 36(15) ps for 0 and 2 kOe, respectively, well within the range typical for SCMs [11,12]. The respective Δ_τ/k_B values were 48.4(1.2) and 44.9(1.0) K. Application of DC field results in slight lowering of the energy barrier, which has been observed for other metamagnetic SCMs [95]. The calculated value of the activation energy $\Delta_A = \Delta_\tau - 2\Delta_\xi$ is close to zero.

Preprints (www.preprints.org) | NOT PEER-REVIEWED | Posted: 9 February 2017 doi:10.20944/preprints201702.0029.v1

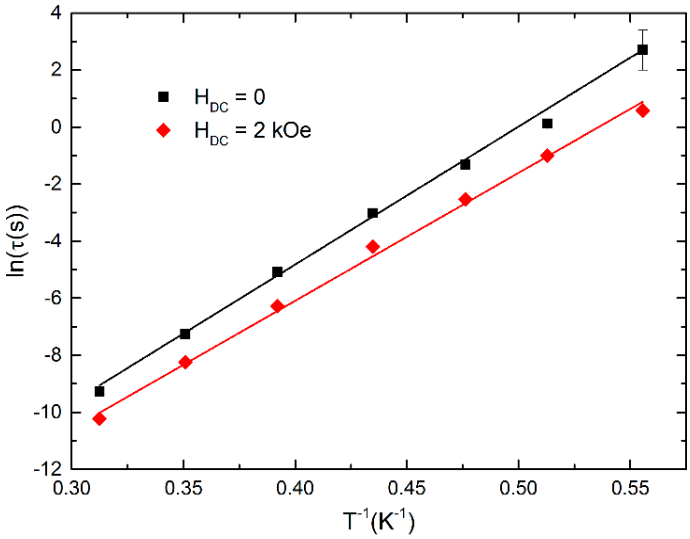

Figure 7. Arrhenius plots of ln(τ) versus T^{-1} for **2** derived from the generalized Debye model fits to the data in 0 and 2 kOe DC fields. Solid lines represent linear fits.

3. Experimental Section

3.1. General Details

All chemical reagents and solvents were purchased from Alfa or Sigma-Aldrich and used without further purification. [Mn(5-TMAMsalen)(H_2O)$_2$](ClO_4)$_3$ ·H_2O [99] and K_3[W(CN)$_8$](H_2O)$_2$ [100,101] were prepared using published procedures. Elemental (C, H, N) analyses were carried out by standard methods with a "Euro-Vector 3000" analyzer. FTIR spectra were measured with a NICOLET instrument in the 4000–375 cm^{-1} range. Thermogravimetric measurements were performed by means of 50 Thermobalance TG 209 F1 Iris® NETZSCH in He (70 ml/min), Al_2O_3 crucible, sample weight ~ 5 mg, heating rate - 10.0 K/min, temperature range 25 – 350 °C. The experiment results were treated using standard software [102]. Powder X-ray measurements were performed using Cu-Kα radiation (λ = 1.5418 Å) with an X'Pro powder diffractometer (PANalytical Inc., Almelo, The Netherlands) at room temperature.

3.2. Magnetic Measurements

All measurements of magnetic properties were performed using a Quantum Design MPMS 5XL SQUID magnetometer in the range of temperatures 1.8 - 300 K and magnetic field up to 50 kOe.

3.3. Single-Crystal X-ray Diffraction

SCXRD studies of **1** were carried out by means of an Xcalibur Ruby Gemini diffractometer at 293 K using graphite-monochromated Mo-Kα radiation (λ = 0.71073 Å). The intensity data were integrated using the related analysis software [103]. An absorption correction based on the crystal faces was applied to the data sets (analytical) [104]. The structure of **1** was solved by direct methods using the SIR^{97} program [105] combined with Fourier difference syntheses and refined against F using reflections with [$I/\sigma(I)$ > 3] by using the CRYSTALS program [106]. All atomic displacement parameters for non-hydrogen atoms were refined with anisotropic terms. The hydrogen atoms were theoretically located based on the conformation of the supporting atom and refined by using the riding model. Selected crystallographic data are presented in Table 3.

Table 3. Crystallographic data and structure refinement summary for **1**.

Preprints (www.preprints.org) | NOT PEER-REVIEWED | Posted: 9 February 2017 doi:10.20944/preprints201702.0029.v1

Formula	$C_{34}H_{43}MnN_{13}O_{5.75}W$
Formula Weight	964.58
Crystal System	triclinic
Space Group	$P\bar{1}$
Lattice Parameters	
a (Å)	11.1881(4)
b (Å)	12.7756(5)
c (Å)	18.5278(8)
α(º)	89.805(3)°
β (º)	74.570(4)°
γ(º)	72.773(3)°
V (Å^3)	2430.09 (17)
Z	2
D_{calc} (g cm^3)	1.318
F(000)	966
λ (Mo Kα) Å	0.71069
l (Mo Ka) (mm^{-1})	2.67
No. of Reflection	
Measured	
Total:	20799
Unique:	11156
reflections with $I > 2.0\sigma(I)$	9319
	R_{int} = 0.037
No.Variables	506
wR_2 (All reflections)[b]	0.055
$R[F^2 > 2\sigma(F^2)]$	0.053
Flack Parameter	
Goodness-of-fit (GOF)	0.9

3.4. Synthetic Details

3.4.1. Synthesis of Complex **1**, $[Mn(5TMAMsalen)(H_2O)][W(CN)_8](H_2O)_{4.75}(CH_3CN)$

The complex was obtained by layering of the constituent solvents. A solution of $K_3[W(CN)_8](H_2O)_2$ (25 mg, 0.05 mmol) in water (8 mL) was divided into four portions, which were placed in narrow diameter (5 mm) glass tubes. Aliquots (2 mL) of a 1:3 mixture of water/acetonitrile were layered on top of the portions of $K_3[W(CN)_8](H_2O)_2$ solution as a dividing buffer layer. This provided a slow diffusion from a third, top layer, consisting of a 2 mL aliquot of a solution of $[Mn(5TMAMsalen)(H_2O)_2]$ $(ClO_4)_3(H_2O)$ (41 mg, 0.05 mmol) in acetonitrile (8 mL). These glass tubes were each capped by parafilm and left undisturbed for three weeks in the dark until elongated block-shaped brawn-green crystals of **1** had formed. Yield: 86.5%. $C_{34}H_{43}MnN_{13}O_{5.75}W$ (964.57) calcd. C 42.34, H 4.49, N 18.88; found C 42.54, H 4.53, N 19.00. IR: ν = 3417.6, 3035.4, 1978.6, 1615.4, 1544.2, 1470.5, 1438.5, 1384.4, 1328.4, 1298.0, 1257.0, 1235.4, 1173.1, 1148.3, 1092.6, 1049.1, 977.1, 919.4, 880.1, 851.8, 832.9, 818.8, 795.9, 759.9, 738.2, 674.0, 636.0, 603.3, 570.3, 496.8, 465.5 cm^{-1}.

3.4.1. Synthesis of Complex **2**, $[Mn(5TMAMsalen)W(CN)_8](H_2O)_8(CH_3CN)$.

To a stirred light yellow solution of $K_3[W(CN)_8](H_2O)_2$ (25 mg, 0.05 mmol) in H_2O (2.5 mL) was added dropwise a dark brown solution of $[Mn(5TMAMsalen)(H_2O)_2](ClO_4)_3(H_2O)$ (41 mg, 0.05 mmol) in acetonitrile (2.5 mL). The precipitated product was stirred for a few minutes at 70 ^{0}C, and then collected by filtration. The solid was washed twice with H_2O (2 mL), twice with MeCN (2 mL) and once with Et_2O (2 mL) and then air-dried. Yield: 97%. IR (KBr): ν = 3306, 2956, 2870, 2380, 1645, 1449, 1115, 535, 475 cm^{-1}. $C_{34}H_{51}MnN_{13}O_{10}W$ (1040.63) calcd. C 39.24, H 4.94, N 17.49; found C 39.25, H 4.92, N 17.52. IR: ν = 3443.8, 3039.5, 1980.5, 1614.6, 1544.2, 1470.4, 1415.1, 1386.2, 1334.2, 1293.1,

Preprints (www.preprints.org) | NOT PEER-REVIEWED | Posted: 9 February 2017 doi:10.20944/preprints201702.0029.v1

1257.0, 1235.2, 1203.3, 1172.9, 1147.7, 1092.3, 1051.0, 998.9, 974.7, 918.0, 878.0, 850.2, 830.7, 818.7, 796.5, 762.9, 736.4, 678.5, 637.0, 604.6, 572.2, 497.4, 467.0 cm^{-1}

Compound **2** was also obtained from **1**: finely ground **1** (35 mg, 0.036 mmol) was dissolved in hot acetonitrile (7 mL). To this solution, distilled water (2 mL) was added. A brown powder was formed after 5 min of stirring with continuous stirring. The precipitate was separated by centrifugation, washed twice with H_2O (2 mL), once with MeCN (2 mL) and once with Et_2O (2 mL) and, then, dried under vacuum. Yield: 89%. According to elemental analysis, the sample obtained from **1** contains less solvated water molecules compared to that prepared from the non-dimerized the constituents. $C_{34}H_{45}MnN_{13}O_6W$ (970.58) calcd. C 42.07, H 4.67, N 18.76; found C 42.10, H 4.72, N 18.67.

4. Conclusions

Apparently, both studied complexes have a different organization in the solid state, as it is evident from their diffractograms (Figure S3, SI). If for **1** their molecular structure was determined form SCXRD date, then a lack of the single crystal structure for **2** does not permit us to explain definitely why the magnetic behavior of this compound is so different compared with **1**. However, our conclusion that **2** is a 1D coordination chain is based on a totality of the experimental facts. At first, the compound **2**, having a ratio $[Mn(SB^+)]^{3+}$ / $[W(CN)_8]^{3-}$ = 1:1, is insoluble in any solvent and can be obtained from **1** (See experimental section). These three features, taken together, support a polymeric character of **2**. At second, for the majority of ν_{CN} peaks in the IR spectrum of **2** is slightly shifted towards higher frequencies compared to those of **1**. Further, the first is somewhat more thermally stable than the latter. Two previous ascertainings are also consistent with a more linked character of $[W(CN)_8]^{3-}$ metalloligand in the chain. At third, magnetic properties of the compound both the static and dynamic do not contradict the proposed structure.

An intriguing difference in character of the spin coupling between the magnetic centers in **1** and **2** is certainly caused by a dissimilarity of their molecular structures in general and geometry of the dimeric W-CN-Mn unit particularly. To clarify this situation we continue a challenge of the single crystal growing to elucidate the structure of **2**.

In summary, the two low dimensional constructed by $[W(CN)_8]^{3-}$ and anisotropic Mn^{III} Schiff base complex have been prepared and characterized. These two compounds are the first examples of the neutral species among a small family of heterobimetallic compounds involving octacyanotungstate(V) as a metalloligand.

Supplementary Materials: Figure S1: TG data for 1 (and 2, Figure S2: DTG data for 1 and 2, Figure S3: (a) diffractograms for 1: experimental (red), simulated (black); simulated for 1 and 2, Figure S4: Zero field–cooling/field cooling χ vs T for 1 (H=20 Oe), Figure S5: AC susceptibility versus temperature for 1. H_{AC}=3 Oe, f_{AC}=10 Hz, Figure S6: The molecular structure of $[(MnSB^+(H_2O)]_2$ dimer in compound I. The O…H hydrogen bonds mediating spin coupling between two Mn^{III} ions, Figure S7: Zero-field cooling and field cooling magnetic susceptibility versus temperature for 2 measured in a DC field of 15 Oe, Figure S8: AC susceptibility versus temperature for 2 measured in H_{DC} = 0 Oe and H_{AC} = 3 Oe at f=10 Hz, Figure S9: AC susceptibility of 2 as a function of temperature measured over a series of AC frequencies in a) zero DC field and b) DC field of 2 kOe, Figure S10: AC susceptibility of **2** as a function of H_{DC} at four temperatures; a) χ', b) χ''. f_{AC}=10 Hz, H_{AC} = 3 Oe, Figure S11: AC susceptibility of 2 measured as a function of AC frequency over a range of temperatures in a) 0 and b) 2 kOe DC field, Table S1: Parameters τ and α obtained from the generalized Debye model fits to the AC data vs. frequency for sets measured in 0 and 2 kOe DC field.

Acknowledgments: This work was supported by the Russian Foundation for Basic Research under grant number 16-03-00880-a and Research Executive Agency under PIIFR-GA-2011-911689. We are grateful to Dr Michał Rams for his help in collection and analysis of the magnetic measurements data.

Author Contributions: Kira E. Vostrikova conceived, designed and performed the chemical experiment, as well as wrote the paper; Guillaume Pilet performed a crystallographic study and participated in the article redaction. Anna M. Majcher collected and fitted the majority of magnetic data, Vladimir S. Mironov contributed to the theoretical estimation of interdimer magnetic interaction for compound **1**.

Conflicts of Interest: The authors declare no conflict of interest

References

1. Gatteschi, D.; Sessoli, R.; Villain, J. *Molecular Nanomagnets*, Oxford University Press: Oxford, Great Britain, 2006; pp. 1–408. 10.1093/acprof:oso/9780198567530.001.0
2. Coulon, C.; Miyasaka, H.; Clérac, R. Single-Chain Magnets: Theoretical Approach and Experimental Systemsin. In *Structure and Bonding*, Winpenny, R., Ed.; Springer-Verlag: Berlin Heidelberg, Germany, 2006, 163–206. doi 10.1007/430_030
3. Bogani, L.; Wernsdorfer, W. Molecular spintronics using single-molecule magnets *Nat. Mater.* 2008, 7, 179-186. 10.1038/nmat2133
4. Molecular Magnets: Physics and Applications, in *NanoScience and Technology,* Juan, B.; Fernando, L.; Fernández, J.F., Eds.; Springer-Verlag: Berlin Heidelberg, Germany, 2014, pp. 1–395. doi 10.1007/978-3-642-40609-6
5. Lescouëzec, R.; Toma, L. .; Vaissermann, J.; Verdaguer, M.; Delgado, F.S.; Ruiz-Pérez, C.; Lloret, F.; Julve, M. Design of single chain magnets through cyanide-bearing six-coordinate complexes. *Coord. Chem. Rev.* **2005**, 249, 2691–2729. doi 10.1016/j.ccr.2005.09.017
6. Miyasaka, H; Clerac, R. Synthetic Strategy for Rational Design of Single-Chain Magnets. *Bull. Chem. Soc. Jap.* **2005**, 78, 1725–1748. doi 10.1246/bcsj.78.1725
7. Miyasaka, H.; Julve, M.; Yamashita, M.; Clérac, R. Slow Dynamics of the Magnetization in One-Dimensional Coordination Polymers: Single-Chain Magnets. *Inorg. Chem.* **2009**, 48, 3420–3437. doi 10.1021/ic802050j
8. Sun, H.-L.; Wang, Z.-M.; Gao, S. Strategies towards single-chain magnets. *Coord. Chem. Rev.* **2010**, 254, 1081–1100. doi 10.1016/j.ccr.2010.02.010
9. Wang, S.; Ding, X.-H.; Li, Y.-H.; Huang, W. Dicyanometalate chemistry: A type of versatile building block for the construction of cyanide-bridged molecular architectures. *Coord. Chem. Rev*, **2012**, 256, 439–464. doi 10.1016/j.ccr.2011.10.029
10. Kang, L.-C.; Zuo, J.-L. *Multifunctional Molecular Materials*, Ouahab, L., Ed.; Pan Stanford Publishing: Singapour, **2013**; 105–131.
11. Zhang, W.-X.; Breedlove, B.; Ishikawa, R.; Yamashita, M. Single-chain magnets: beyond the Glauber model. *RSC Advances* **2013**, *3*, 3772–3798; doi 10.1039/C2RA22675H
12. Gatteschi, D.; Vindigni, A. Single-Chain Magnets. In *Molecular Magnets;* Springer-Verlag: Berlin Heidelberg, Germany, 2014, pp. 191–220. doi 10.1007/978-3-642-40609-6_8
13. Ishikawa, R.; Katoh, K.; Breedlove, B. K; Yamashita, M. Mn^{III}(tetrabiphenylporphyrin)–TCNE Single-Chain Magnet via Suppression of the Interchain Interactions. *Inorg. Chem.* **2012**, 51, 9123–9131. doi 10.1021/ic3015223
14. Bhargavi, G.; Rajasekharan, M.V.; Costes, J.-P.; Tuchagues, J.-P. A new end-on azido bridged MnIII single-chain magnet and its dimeric single molecule magnet polymorph. Synthesis, structure and magnetic properties of $[Mn(5\text{-}Clsalpn)N_3]_n$ and phenoxo bridged $[Mn(5\text{-}Clsalpn)N_3]_2$. *Dalton Trans.* **2013**, 42, 8113–8123. doi 10.1039/C3DT31966K
15. Senapati, T.; Pichon, C.; Ababei, R.; Mathoniere, C.; Clérac, R. Cyanido-Bridged Fe(III)–Mn(III) Heterobimetallic Materials Built From Mn(III) Schiff Base Complexes and Di- or Tri-Cyanido Fe(III) Precursors. *Inorg. Chem.* **2012**, 51, 3796–3812. doi 10.1021/ic2027708
16. Boeckmann, J.; Wriedt, M.; Näther, C. Metamagnetism and Single-Chain Magnetic Behavior in a Homospin One-Dimensional Iron(II) Coordination Polymer. *Chem. Eur. J.* **2012**, 18, 5284–5289. doi 10.1002/chem.201103416
17. Zhang, W.-X.; Shiga, T.; Miyasaka, H.; Yamashita, M. New Approach for Designing Single-Chain Magnets: Organization of Chains via Hydrogen Bonding between Nucleobases. *J. Am. Chem. Soc.* **2012**, 134, 6908–6911. doi 10.1021/ja300152k.
18. Sahoo, S.; Sutter, J.-P.; Ramasesha, S. Study of Low Temperature Magnetic Properties of a Single Chain Magnet with Alternate Isotropic and Non-collinear Anisotropic Units. *J. Stat. Physics* **2012**, 147, 181–193. doi 10.1007/s10955-012-0460-7
19. Liu, R.N.; Hu, P.; Li, L.C.; Liao, D.Z.; Sutter, J.-P. One-dimensional lanthanide complexes bridged by nitronyl nitroxide radical ligands with non-chelating nitrogen donors: Structure and magnetic characterization. *Sci. China Chem.* **2012**, 55, 997–1003. doi 10.1007/s11426-012-4580-3

20. Li, Z.-X.; Jie, W.; Zha, G.; Wang, T.; Xu, Y. Nitrate-Templated 1D EE-Azide-Cobalt Chain Exhibits Canted Antiferromagnetism and Slow Magnetic Relaxation. *Eur. J. Inorg. Chem.* **2012**, 22, 3537–3540. doi 10.1002/ejic.201200445
21. Liu, R.; Xiong, C.; Zhao, S.; Wu, J.; Li, Q.; Fang, D. Ruthenium (II) complexes binding to human serum albumin and inducing apoptosis of tumor cells. *Inorg. Chem. Comm.* **2012**, 22, 104–107. doi 10.1016/j.inoche.2012.08.009
22. Tomkowicz, Z.; Rams, M.; Balanda, M.; Foro, S.; Nojiri, H.; Krupskaya, Y.; Kataev, V.; Buchner, B.; Nayak, S.K.; Yakhmi, J.V.; Haase, W. Slow Magnetic Relaxations in Manganese(III) Tetra(meta-fluorophenyl)porphyrin-tetracyanoethenide. Comparison with the Relative Single Chain Magnet ortho Compound. *Inorg. Chem.* **2012**, 51, 9983–9994. doi 10.1021/ic3014
23. Hoshino, N.; Iijima, F.; Newton, G.N.; Yoshida, N.; Shiga, T.; Nojiri, H.; Nakao, A.; Kumai, R.; Murakami, Y.; Oshio, H. Three-way switching in a cyanide-bridged [CoFe] chain. *Nature Chem.* **2012**, 4, 921–926. doi 10.1038/nchem.1455
24. Visinescu, D.; Jeon, I.-R.; Madalan, A.M.; Alexandru, M.-G.; Jurca, B.; Mathoniere, C.; Clérac, R.; Andruh, M. Self-assembly of $[Cu^{II}Tb^{III}]^{3+}$ and $[W(CN)_8]^{3-}$tectons: a case study of a mixture containing two complexes showing slow-relaxation of the magnetization. *Dalton Trans.* **2012**, 41, 13578–13581. doi 10.1039/C2DT32081A
25. Yao, M.-X.; Zheng, Q.; Qian, K.; Song, Y.; Gao, S.; Zuo, J.-L. Controlled Synthesis of Heterotrimetallic Single-Chain Magnets from Anisotropic High-Spin 3d–4f Nodes and Paramagnetic Spacers. *Chem. Eur. J.* **2013**, 19, 294–303. doi 10.1002/chem.201203361
26. Mougel, V.; Chatelain, L.; Hermle, J.; Caciuffo, R.; Colineau, E.; Tuna, F.; Magnani, N.; Degeyer, A; Pécaut J.; Mazzanti, M. A Uranium-Based UO^{2+}–Mn^{2+} Single-Chain Magnet Assembled trough Cation–Cation Interaction. *Angew. Chem. Int*. **2014**, 53, 819–823. 10.1002/anie.201307366
27. Vaz, M. G.F.; Cassaro, R.A.A.; Akpinar, H.; Schlueter, J.A.; Lahti, P.M.; Novak, M.A. A Cobalt Pyrenylnitronylnitroxide Single-Chain Magnet with High Coercivity and Record Blocking Temperature *Chem. Eur. J.* **2014**, 20, 5460–5467. doi 10.1002/chem.201304852.
28. Glauber, R. J. Time-Dependent Statistics of the Ising Model. *J. Math. Phys.*, 1963, **4**, 294–307. doi 10.1063/1.1703954
29. Suzuki, M.; Kubo, R. Dynamics of the Ising Model near the Critical Point. *J. Phys. Soc. Jpn*. **1968**, 24, 51–60. doi 10.1143/JPSJ.24.51
30. Coulon, C.; Clérac, R.; Lecren, L.; Wernsdorfer, W.; Miyasaka, H. Glauber dynamics in a single-chain magnet: From theory to real systems. *Phys. Rev. B* **2004**, 69, 132408. doi 10.1103/PhysRevB.69.132408
31. Miyasaka, H.; Saitoh, A.; Abec, S. Magnetic assemblies based on Mn(III) salen analogues. *Coord. Chem. Rev.* **2007**, 251, 2622–2664. doi 10.1016/j.ccr.2007.07.028
32. Wang, X.-Y.; Avendaño, C.; Dunbar, K. R. Molecular magnetic materials based on 4d and 5d transition metals. *Chem. Soc. Rev.* **2011**, 40, 3213–3238. Doi 10.1039/C0CS00188K
33. Dreiser, J.; Pedersen, K.S.; Schnegg, A.; Holldack, K.; Nehrkorn, J.; Sigrist, M.; Tregenna-Piggott, P.; Mutka, H.; Weihe, H.; Mironov, V.S.; Bendix, J.; Waldmann, O. Three-Axis Anisotropic Exchange Coupling in the Single-Molecule Magnets $NEt_4[Mn^{III}_2(5\text{-Brsalen})_2(MeOH)_2M^{III}(CN)_6]$ (M=Ru, Os). *Chem. Eur. J.* **2013**, 19, 3693–3701. doi 10.1002/chem.201203781
34. Qian, K.; Huang, X.-C.; Zhou, C.; You, X.-Z.; Wang, X.-Y.; Dunbar, K. R. A Single-Molecule Magnet Based on Heptacyanomolybdate with the Highest Energy Barrier for a Cyanide Compound. *J. Am. Chem. Soc.* **2013**, 135, 13302–13305. doi 10.1021/ja4067833
35. Miyasaka, H.; Saitoh, A.; Yamashita, M.; Clérac, R. A $Mn^{III}_2Ni^{II}$ single-chain magnet separated by a thick isolating network of BPh_4^- anions *Dalton Trans.* **2008**, 2422–2427. doi 10.1039/B718036E
36. Choi, H.J.; Sokol, J.J.; Long, J.R. Raising the Spin-Reversal Barrier in Cyano-Bridged Single-Molecule Magnets: Linear $Mn^{III}_2M^{III}(CN)_6$ (M=Cr, Fe) Species Incorporating $[(5\text{-Brsalen})Mn]^+$ Units *Inorg. Chem.* **2004**, 43, 1606–1608. doi 10.1021/ic035327q
37. Miyasaka, H.H.; Takahashi, Madanbashi, T.; Sugiura, K.; Clérac, R.; Nojiri, H. Cyano-Bridged $Mn^{III}_3M^{III}$ (M^{III} = Fe, Cr) Complexes: Synthesis, Structure, and Magnetic Properties. *Inorg. Chem.* **2005**, 44, 5969–5971. doi 10.1021/ic0505753
38. Tregenna-Piggott, P.L.W.; Sheptyakov, D.; Keller, L.; Klokishner, S.I.; Ostrovsky, S.M.; Palii, A.V.; Reu, O.S.; Bendix, J.; Brock-Nannestad, T.; Pedersen, K.; Weihe, H.; Mutka, H. Single-Ion Anisotropy and Exchange Interactions in the Cyano-Bridged Trimers $Mn^{III}_2M^{III}(CN)_6$ (M^{III} = Co, Cr, Fe) Species

Incorporating [Mn(5-Brsalen)]$^{+}$ Units: An Inelastic Neutron Scattering and Magnetic Susceptibility Study *Inorg. Chem.* **2009**, 48, 128–134. doi 10.1021/ic801727p

39. Feng, X.W.; Liu, J.; Harris, T.D.; Hill, S.; Long, J.R. Slow Magnetic Relaxation Induced by a Large Transverse Zero-Field Splitting in a $Mn^{II}Re^{IV}(CN)_2$ Single-Chain Magnet. *J. Am. Chem. Soc.* **2012**, 134, 7521-7529. doi 10.1021/ja301338d
40. Li, Y.-H.; He, W.-R.; Ding, X.-H.; Wang, S.; Cui, L.-F.; Huang, W. Cyanide-bridged assemblies constructed from capped tetracyanometalate building blocks $[M_A(ligand)(CN)_4]^{1-/2-}$($M_A$ = Fe or Cr) *Coord. Chem. Rev.* **2012**, 256, 2795–2815. doi 10.1016/j.ccr.2012.09.014
41. Toma, L.M.; Pasan, J.; Catalina R.-P.; Julve, M.; Lloret, F. $[Fe^{III}(dmbpy)(CN)_4]^{-}$: a new building block for designing single-chain magnets *Dalton Trans.*, **2012**, 41, 13716–13726. doi 10.1039/C2DT31675G
42. Kang, S.; Kanegawa, S.; Sato, O. Slow magnetic relaxation in a 4,2-ribbon like $Fe^{III}_2Co^{II}$ heterobimetallic chain. *Dalton Trans.*, **2012**, 41, 13575–13577. doi 10.1039/C2DT31168B
43. Dong, D.-P.; Liu, T.; Zheng, H.; Zhao, L.; Zhuang, P.-F.; He, C.; Duan, C.-Y. Synthesis, structures and single chain magnet behavior of a cyano-bridged {Fe_2Cu} chain. *Inorg. Chem., Commun.* **2012**, 24, 153–156. doi 10.1016/j.inoche.2012.08.021
44. Chorazy, S.; Nakabayashi, K.; Imoto, K.; Mlynarski, J.; Sieklucka, B.; Ohkoshi, S. Conjunction of Chirality and Slow Magnetic Relaxation in the Supramolecular Network Constructed of Crossed Cyano-Bridged Co^{II}–W^{V}Molecular Chains. *J. Am. Chem. Soc.* **2012**, 134, 16151–16154. doi 10.1021/ja307520k
45. Toma, L.M.; Ruiz-Perez, C.; Pasan, J.; Wernsdorfer, W.; Lloret, F; Julve, M. Molecular Engineering To Control the Magnetic Interaction between Single-Chain Magnets Assembled in a Two-Dimensional Network *J. Am. Chem. Soc.*, **2012**, 134, 15265–15268. doi 10.1021/ja307042z
46. Bhowmick, I.; Hillard, E.A.; Dechambenoit, P.; Coulon, C.; Harris, T.D.; Clérac, R. A canted antiferromagnetic ordered phase of cyanido-bridged $Mn^{III}2Re^{IV}$ single-chain magnets *Chem. Commun.* **2012**, 48, 9717–9719. doi 10.1039/C2CC34066F
47. Ferbinteanu, M.; Miyasaka, H.; Wernsdorfer, W.; Nakata, K.; Sugiura, K.; Yamashita, M.; Coulon, C.; Clérac, R. Single-Chain Magnet $(NEt_4)[Mn_2(5\text{-}MeOsalen)_2Fe(CN)_6]$ Made of Mn^{III}-Fe^{III}-Mn^{III} Trinuclear Single-Molecule Magnet with an ST) 9/2 Spin Ground State *J. Am. Chem. Soc.* **2005**, 127, 3090–3099. doi 10.1021/ja0468123
48. Miyasaka, H.; Madanbashi, T.; Saitoh, A.; Motokawa, N.; Ishikawa, R.; Yamashita, M.; Bahr, S.; Wernsdorfer, W.; Clérac, R. Cyano-Bridged $Mn^{III}M^{III}$ Single-Chain Magnets with M^{III}=Co^{III}, Fe^{III}, Mn^{III}, and Cr^{III} *Chem. Eur. J.* **2012**, 18, 3942–3954. doi 10.1002/chem.201102738
49. Bleuzen, A.; Marvaud, V.; Mathoniere, C.; Sieklucka; B.; Verdaguer, M. Photomagnetism in Clusters and Extended Molecule-Based Magnets. *Inorg. Chem.*, **2009**, *48*, 3453–3466. **doi** 10.1021/ic802007g
50. Sieklucka, B.; Podgajny, R.; Przychodzen, P.; Korzeniak, T. Engineering of octacyanometalate-based coordination networks towards functionality. *Coord. Chem. Rev.*, **2005**, *249*, 2203–2220. doi 10.1016/j.ccr.2005.02.024
51. Przychodzen, P.; Korzeniak, T.; Podgajny, R.; Sieklucka, B. Supramolecular coordination networks based on octacyanometalates: From structure to function. *Coord. Chem. Rev.*, **2006**, *250*, 2234–2260. doi 10.1016/j.ccr.2006.01.026
52. Sieklucka, B.; Podgajny, R.; D. Pinkowicz, B. Nowicka, Korzeniak, T.; Bałanda, M.; Wasiutyński, T.; Pełka, R.; Makarewicz, M.; Czapla, M.; Rams, M.; Gaweł B.B.; Łasocha, W. Towards high T_c octacyanometalate-based networks. *CrystEngComm*, **2009**, 11, 2032–2039. doi 10.1039/B905912A
53. You, Y.S.; Kim, D.; Do, Y.; Oh, S.J.; Hong, C. S. One-Dimensional Octacyanomolybdate-Based Cu(II)−Mo(V) Bimetallic Assembly with a Novel Rope-Ladder Chain Structure. *Inorg. Chem.*, **2004**, *43*, 6899–6901. doi 10.1021/ic048856i
54. Yoon, J.H.; Lee, J.W.; Ryu, D.W.; Choi, S.Y.; Yoon, S.W.; Suh, B.J.; Koh, E.K.; Kim, H.C.; Hong, C.S. Cyanide-Bridged $W^{V}Mn^{III}$ Single-Chain Magnet with Isolated Mn^{III} Moieties Exhibiting Two Types of Relaxation Dynamics *Inorg. Chem.* **2011**, 50, 11306–11308. doi 10.1021/ic202100y
55. Yoo, H.S.; Ko, H.H.; Ryu, D.W.; Lee, J.W.; Yoon, J.H.; Lee, W.R.; Kim, H.C.; Koh, E.K.; Hong, C.S. Octacyanometalate-Based Ferrimagnetic $M^{V}Mn^{III}$ (M = Mo, W) bimetallic chain racemates with slow magnetic relaxations, *Inorg. Chem.* **2009**, *48*, 5617–5619. doi 10.1021/ic900879d
56. Yoon, J.H.; Lim, K.S.; Ryu, D.W.; Lee, W.R.; Yoon, S.W.; Suh, B.J.; Hong, C.S. Synthesis, Crystal Structures, and Magnetic Properties of Cyanide-Bridged $W^{V}Mn^{III}$ Anionic Coordination Polymers Containing Divalent Cationic Moieties: Slow Magnetic Relaxations and Spin Crossover Phenomenon *Inorg. Chem.*, **2014**, *53*, 10437–10442; doi 10.1021/ic501506s

57. Kou, H.-Z.; Ni, Z.-H.; Zhou, B.C.; Wang, R.-J.; Kou, H.-Z.; Ni, Z.-H.; Zhou, B.C.; Wang, R.-J. A cyano-bridged molecule-based magnet containing manganese(III) Schiff base and octacyanotungstate(V) building blocks, *Inorg. Chem. Commun.* **2004**, 7, 1150–1153. doi 10.1021/ic202100y
58. Lim, J.H.; Kang, J.S.; Kim, H.C.; Koh, E.K.; Hong, C.S. Synthesis, Crystal Structures, and Magnetic Properties of Cyano-Bridged Honeycomblike Layers M^{V}–Cu^{II} (M = Mo, W) Chelated by a Macrocyclic Ligand *Inorg. Chem*. **2006**, *45*, 7821–2787. doi 10.1021/ic060868b
59. Nowicka, B.; Rams, M.; Stadnicka, K.; Sieklucka, B. Reversible Guest-Induced Magnetic and Structural Single-Crystal-to-Single-Crystal Transformation in Microporous Coordination Network $\{[Ni(cyclam)]_3[W(CN)_8]_2\}_n$ *Inorg. Chem.* **2007**, *46*, 8123–8125. doi 10.1021/ic701168x
60. Nowicka, B.; Bałanda, M.; Gaweł, B.; Ćwiak, G.; Budziak, A.; Łasocha; W.; Sieklucka, B. Microporous $\{[Ni(cyclam)]_3[W(CN)_8]_2\}_n$ affording reversible structural and magnetic conversions *Dalt. Trans.*, **2011**, *40*, 3067–3073. doi 10.1039/C0DT01434F
61. Larionova, J. ; Clerac, R.; Donnadieu, B.; Willemin, S.; Guerin C. Synthesis and Structure of a Two-Dimensional Cyano-Bridged Coordination Polymer $[Cu(cyclam)]_2[Mo(CN)_8]\cdot 10.5H_2O$ (Cyclam = 1,4,8,11-Tetraazacyclodecane). *Cryst. Gr. Des.*, **2003**, *3*, 267–272. doi 10.1021/cg020048j
62. Umeta, Y.; Tokoro, H.; Ozaki, N.; Ohkoshi, S. Room-temperature thermally induced relaxation effect in a two-dimensional cyano-bridged Cu-Mo bimetal assembly and thermodynamic analysis of the relaxation process *AIP ADVANCES*, **2013**, *3*, 042133. doi 10.1063/1.4802970
63. Venkatakrishnan, T.S.; Sahoo, S.; Bréfuel, N.; Duhayon, C.; Paulsen, C.; Barra, A.-L.; Ramasesha, S.; Sutter, J.-P. Enhanced ion anisotropy by nonconventional coordination geometry: single-chain magnet behavior for a $[\{Fe^{II}L\}_2\{Nb^{IV}(CN)_8\}]$ helical chain compound designed with heptacoordinate Fe^{II}, *J. Am. Chem. Soc.* **2010**, *132*, 6047–6056. doi 10.1021/ja9089389
64. Sieklucka, B.; Podgajny, R.; Korzeniak, T.; Nowicka, B.; Pinkowicz, D.; Kozieł, M. A decade of octacyanides in polynuclear molecular materials, *Eur. J. Inorg. Chem.*, **2011**, 3, 305–326. doi 10.1002/ejic.201190003
65. Ohkoshi, S.; Hashimoto, K. Photo-magnetic and magneto-optical effects of functionalized metal polycyanides, *J. Photochem. Photobio. C: Photochem. Rev.* **2001**, *2*, 71–88. doi 10.1016/S1389-5567(01)00011-9
66. Pinkowicz, D.; Pełka, R.; Drath, O.; Nitek, W.; Bałanda, M.; Majcher, A.M.; Poneti G.; Sieklucka B. Nature of Magnetic Interactions in 3D $\{[M^{II}(pyrazole)_4]_2[Nb^{IV}(CN)_8]\cdot 4H_2O\}_n$ (M = Mn, Fe, Co, Ni) Molecular Magnets *Inorg. Chem.*, **2010**, *49*, 7565-7576. doi 10.1021/ic100937h
67. Qian, J.; Hu, J.; Zhang, J.; Yoshikawa, H.; Awaga, K.; Zhang C. Solvent-Induced Assembly of Octacyanometalates-Based Coordination Polymers with Unique *afm*1 Topology and Magnetic Properties *Cryst. Growth Des.* **2013,** *13*, 5211–5219. doi 10.1021/cg400909b
68. Pinkowicz, D.; Podgajny, R.; Nitek, W.; Rams, M.; Majcher, A.M.; Nuida, T.; Ohkoshi, S.; Sieklucka B. Multifunctional Magnetic Molecular $\{[Mn^{II}(urea)_2(H_2O)]_2[Nb^{IV}(CN)_8]\}_n$ System: Magnetization-Induced SHG in the Chiral Polymorph *Chem. Mater.* **2011**, *23*, 21–31. doi 10.1021/cm102388q
69. Przychodzeń, P.; Rams, M.; Guyard-Duhayon, C.; Sieklucka, B. Antiferromagnetic coupling through cyano-bridge and H-bonds in $[Mn^{III}$(3-OMesalophen)$(H_2O)_2]_2[Mn^{III}$(3-OMesalophen)$(H_2O)]$ $[W^{V}(CN)_8]\cdot 2H_2O$, *Inorg. Chem. Commun.* **2005**, 8, 350–354. doi 10.1016/j.inoche.2005.01.024
70. P. Przychodzeń, K. Lewiński, M. Bałanda, R. Pełka, M. Rams, T. Wasiutyński, C. Guyard-Duhayon, B. Sieklucka, Crystal structures and magnetic properties of two low-dimensional materials constructed from $[Mn^{III}(salen)H_2O]^+$ and $[M(CN)_8]^{3-/4-}$ (M = Mo or W) precursors, *Inorg. Chem.* **2004**, 43, 2967–2974. doi 10.1021/ic035464n
71. *Antifer* Yang, C.; Wang, Q.-L.; Su, C.-Y.; Hu, L.-N.; Li, L.-C.; Liao, D.-Z. A W(V)–Mn(III) bimetallic assembly built by manganese(III) Schiff-base and octacyanotungstate(V) building blocks: Structure and magnetic property *Inorg. Chem. Commun.* **2014**, 40, 26–30. doi 10.1016/j.inoche.2013.11.028
72. Wang, T.-W.; Wang, J.; Ohkoshi, S.; Song, Y.; You, X.-Z. Manganese(II)-octacyanometallate(V) bimetallic ferrimagnets with T_c from 41 to 53 K obtained in acidic media, *Inorg. Chem.* **2010**, 49, 7756–7763. doi 10.1021/ic100591h
73. Ohkoshi, S.; Ikeda, S.; Hozumi, T.; Kashiwagi, T.; Hashimoto, K. Photoinduced magnetization with a high curie temperature and a large coercive field in a cyano-bridged cobalt–tungstate bimetallic assembly, *J. Am. Chem. Soc.* **2006**, 128, 5320–5321. doi 10.1021/ja060510e
74. Mathoniére, C.; Podgajny, R.; Guionneau, P.; Labrugere, C.; Sieklucka, B. Photomagnetism in Cyano-Bridged Hexanuclear Clusters $[Mn^{II}(bpy)_2]_4[M^{IV}(CN)_8]_2\cdot xH_2O$ (M = Mo, x = 14, and M = W, x = 9) *Chem. Mater.* **2005,** *17*, 442–449. doi 10.1021/cm048785l

75. Song, Y.; Zhang, P.; Ren, X.-M.; Shen, X.-F.; Li, Y.-Z.; You, X.-Z. Octacyanometalate-based single-molecule magnets: $Co^{II}_9M^{V}_6$ (M = W, Mo), *J. Am. Chem. Soc.* **2005**, 127, 3708–3709. doi 10.1021/ja042334k
76. Nowicka, B.; Korzeniak, T.; Stefańczyk, O.; Pinkowicz, D.; Chorąży, S.; Podgajny, R.; Sieklucka, B. The impact of ligands upon topology and functionality of octacyanidometallate-based assemblies, *Coord. Chem. Rev.* **2012**, 256, 1946–1971. doi 10.1016/j.ccr.2012.04.008
77. Ko, H.H.; Lim, J.H.; Yoo, H.S.; Kang, J.S.; Kim, H.C.; Koh, E.K.; Hong, C.S. Two W^{V}–Mn^{III} bimetallic assemblies built by octacyanotungstate(V) and Mn^{III} Schiff bases: molecular structures and a spin-flop transition *Dalton Trans.*, **2007**, *20*, 2070–2076. doi 10.1039/B701704A
78. Choi, S.W.; Ryu, D.W.; Lee, J.W.; Yoon, J.H.; Kim, H.C.; Lee, H.; Cho, B.K.; Hong, C.S. One-dimensional cyanide-bridged $Mn^{III}W^{V}$ bimetallic complexes: Metamagnetism, spontaneous resolution, and slow magnetic relaxation. *Inorg. Chem.*, **2009**, *48*, 9066–9068. doi 10.1021/ic901610j
79. Choi, S.W.; Kwak, H.Y.; Yoon, J.H.; Kim, H.C.; Koh, E.K.; Hong, C.S. Intermolecular contact-tuned magnetic nature in one-dimensional 3d-5d bimetallic systems: From a metamagnet to a single-chain magnet. *Inorg. Chem.*, **2008**, 47, 10214–10216. doi 10.1021/ic801699p
80. Lee, J.W.; Lim, K.S.; Yoon, J.H.; Ryu, D.W.; Koo, B.H.; Koh, E.K.; Hong, C.S. Cyanide-bridged single molecule magnet based on a manganese(III) complex with TTF-fused Schiff base ligand *Sci. China Chem.*, **2012**, *55*, 1012–1017. doi 10.1007/s11426-014-5177-9
81. Lim, K.S.; Hong, C.S. $[W(CN)_6(L)]^{1-/2-}$ (L = bidentate ligand) as a useful building unit to construct molecule-based magnetic systems. *Dalton Trans.*, **2013**, *42*, 14941-14950. doi 10.1039/C3DT52040D
82. Ishikawa, R.; Nakano, M; Breedlove, B.K.; Yamashita, M. Syntheses, structures, and magnetic properties of discrete cyano-bridged heterodinuclear complexes composed of Mn^{III}(salen)-type complex and $M^{III}(CN)_6$ anion (M^{III} = Fe, Mn, Cr) *Polyhedron,* **2013**, *64*, 346–351. doi 10.1016/j.poly.2013.06.012
83. Kiernan, P.M.; Griffith, W.P. Studies on transition-metal cyano-complexes. Part I. Octacyanoniobates(III), -niobates(IV), -molybdates(V), and -tungstates(V). *J. Chem. Soc., Dalton Trans.*, **1975**, 2489–2494. doi 10.1039/DT9750002
84. Peresypkina, E.V.; Vostrikova, K.E. $2[Mn(acacen)]^{+}$ + $1[Fe(CN)_5NO]^{2-}$ polynuclear heterobimetallic coordination compounds of different dimensionality in the solid state. *Dalton Trans.*, **2012**, *41*, 4100–4106. doi 10.1039/C2DT11983H
85. Rams, M.; Peresypkina, E.V.; Mironov, V.S.; Wernsdorferand, W.; Vostrikova, K.E. Magnetic Relaxation of 1D Coordination Polymers $(X)_2[Mn(acacen)Fe(CN)_6]$, X = Ph_4P^{+}, Et_4N^{+} *Inorg. Chem.*, **2014**, *53*, 10291–10doi: 10.1021/ic501330j
86. Mironov, V.S.; Chibotaru, L.F.; Ceulemans, A. Exchange interaction in the $YbCrBr_9^{3-}$ mixed dimer: The origin of a strong Yb^{3+}–Cr^{3+} exchange anisotropy. *Phys. Rev. B* **2003**, *67*, 014424–014428. doi 10.1103/PhysRevB.67.014424.
87. Zorina, E.N.; Zauzolkova, N.V.; Sidorov, A.A.; Aleksandrov, G.G.; Lermontov, A.S.; Kiskin, M.A.; Bogomyakov, A.S.; Mironov, V.S.; Novotortsev, V.M.; Eremenko, I.L. Novel polynuclear architectures incorporating Co^{2+} and K^{+} ions bound by dimethylmalonate anions: Synthesis, structure, and magnetic properties. *Inorg. Chim. Acta.* **2013**, 396, 108-118. doi 10.1016/j.ica.2012.10.016.
88. Samsonenko, D.G.; Paulsen, C.; Lhotel, E.; Mironov, V.S.; Vostrikova, K.E. $[Mn^{III}$(Schiff base)$]_3[Re^{IV}(CN)_7]$, highly anisotropic 3D coordination framework: synthesis, crystal structure, magnetic investigations, and theoretical analysis. *Inorg. Chem.* **2014**, 53, 10217-10231. doi 10.1021/ic501247x
89. Mironov, V. S. Origin of Dissimilar Single-Molecule Magnet Behavior of Three $Mn^{II}_2Mo^{III}$ Complexes Based on $[Mo^{III}(CN)_7]^{4-}$ Heptacyanomolybdate: Interplay of Mo^{III}–CN–Mn^{II} Anisotropic Exchange Interactions. *Inorg. Chem.* **2015**, 54, 11339–11355. doi 10.1021/acs.inorgchem.5b01
90. Schaffer, C. E. A perturbation representation of weak covalent bonding. The symmetry basis for the angular overlap model of the ligand field. *Struct. Bonding.* **1968**, 5, 68-95. doi 10.1007/BFb0118847.
91. Tokyo Institute of Technology, Dept. Organic & Organic Materials Engineering. Atomic Parameters for Extended Huckel Calculation. Available online: http://www.op.titech.ac.jp/lab/mori/EHTB/EHTB~1.html (accessed on 31.01.2017)
92. Lee, S. Electron localization and the structure of transition metal chains. *J. Am. Chem. Soc.* **1989**, 111, 7754–7761. doi 10.1021/ja00202a015
93. Seiden J., Propriétés statiques d'une chaîne isotrope alternée de spins quantiques 1/2 et de spins classiques. *J. Physique Lett.*, **1983**, *44*, 947–952. doi 10.1051/jphyslet:019830044023094 Note that the intra-chain exchange is written as 2J in this work, which is equal to the coupling constant J introduced by J. Seiden.

94. Carlin, R.L.; Van Duyneveldt, A.J. Magnetic properties of transition metal compounds; Springer Verlag: Berlin, Germany, 1977.
95. Wöhlert, S.; Fic, T.; Tomkowicz, Z.; Ebbinghaus, S.G.; Rams, M.; Haase, W.; Näther, C. Structural and Magnetic Studies of a New Co(II) Thiocyanato Coordination Polymer Showing Slow Magnetic Relaxations and a Metamagnetic Transition. *Inorg. Chem.*, **2013**, *52*, 12947–12957. doi 10.1021/ic4012235
96. Prosvirin, A.V.; Zhao, H.; Dunbar, K.R. A Mn(III) chain derived from Mn_{12}–acetate that exhibits both glauber dynamics and antiferromangetic ordering regimes. *Inorg. Chim. Acta*, **2012**, *389*, 118–121. doi 10.1016/j.ica.2012.03.006
97. Mydosh, J. A. *Spin Glasses: An Experimental Introduction*; Taylor and Francis: London, 1993; p. 67.
98. Cole, K.S.; Cole, R.H. Dispersion and Absorption in Dielectrics I. Alternating Current Characteristics. *J. Chem. Phys.* **1941**, 9, 341. doi 10.1063/1.1750906
99. Sakamoto, F.; Sumiya, T.; Fujita, M.; Tada, T.; Tan, X.S.; Suzuki, E.; Okura, I.; Fujii, Y. T-site selective photocleavage of DNA by cationic Schiff base complex of manganese(III) *Chem. Lett.*, 1998, 1127–1128. doi 10.1246/cl.1998.1127
100. Baadsgaard, H.; Treadwell, W.D. Zur Kenntnis der komplexen Wolframcyanide $K_4[W(CN)_8]$ $2H_2O$ und $K_3[W(CN)_8]$ H_2O. *Helv. Chim. Acta*, **1955**, *38*, 1669–1679. doi 10.1002/hlca.19550380703
101. Goodenow, E.L.; Garner, C.S. The Exchange Reaction between Octacyanotungstate(IV) and Octacyanotungstate(V) Ions, *J. Amer. Chem. Soc.*, **1955, 77,** 5272–5274. doi 10.1021/ja01625a015
102. NETZSCH Proteus Thermal Analysis v.4.8.1.–NETZSCH55 Geratebau – Bayern, Germany. 2005.
103. *CrysAlisPro*, v. 1.171.33.46 (rel. 27-08-2CrysAlis171.NET), Oxford Diffraction Ltd., **2009**.
104. De Meulenaar, J.; Tompa, H. The absorption correction in crystal structure analysis. *Acta Crystallogr.* **1965**, *19*, 1014–1018. doi 10.1107/S0365110X65004802
105. Cascarano, G.; Altomare, A.; Giacovazzo, C.; Guagliardi, A.; Moliterni, A.G.G.; Siliqi, D.; Burla, M.C.; Polidori, G.; Camalli, M. SIRWARE *Acta Crystallogr., Sect. A* **1996**, *52*, C-79. doi 10.1107/S0108767396095943.
106. University of Oxford. Crystallography program «Crystalsv1461». Available online: http://www.xtl.ox.ac.uk/crystals.1.html (accessed on 31.01.2017)

Preprints (www.preprints.org) | NOT PEER-REVIEWED | Posted: 9 February 2017 doi:10.20944/preprints201702.0029.v1

Supporting Information

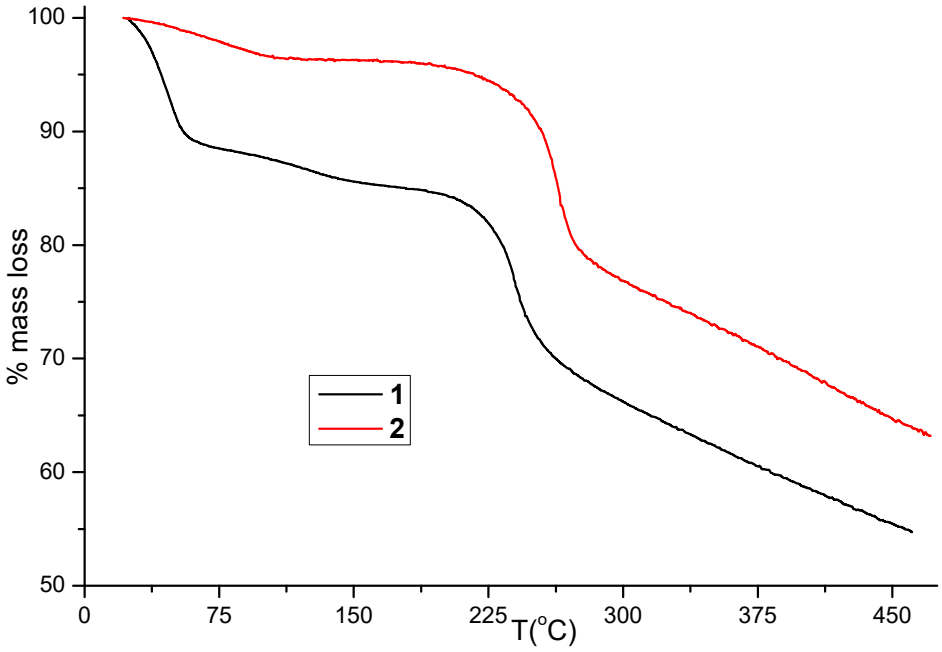

Figure S1 TG data for **1** (black) and **2** (red).

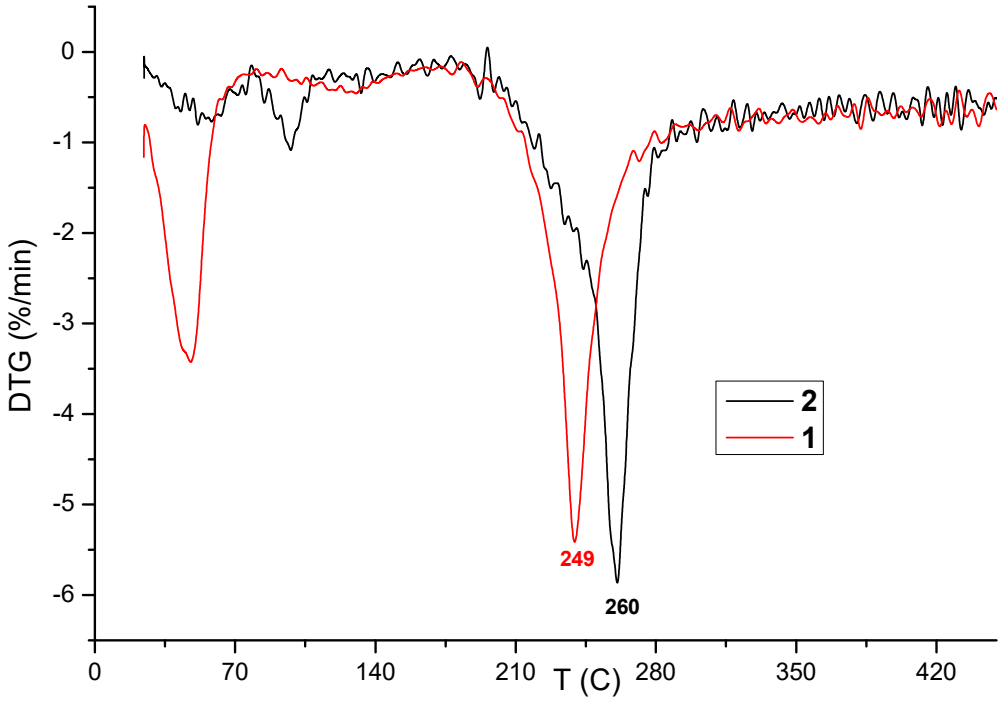

Figure S2. DTG data for **1** (red) and **2** (black).

Preprints (www.preprints.org) | NOT PEER-REVIEWED | Posted: 9 February 2017 doi:10.20944/preprints201702.0029.v1

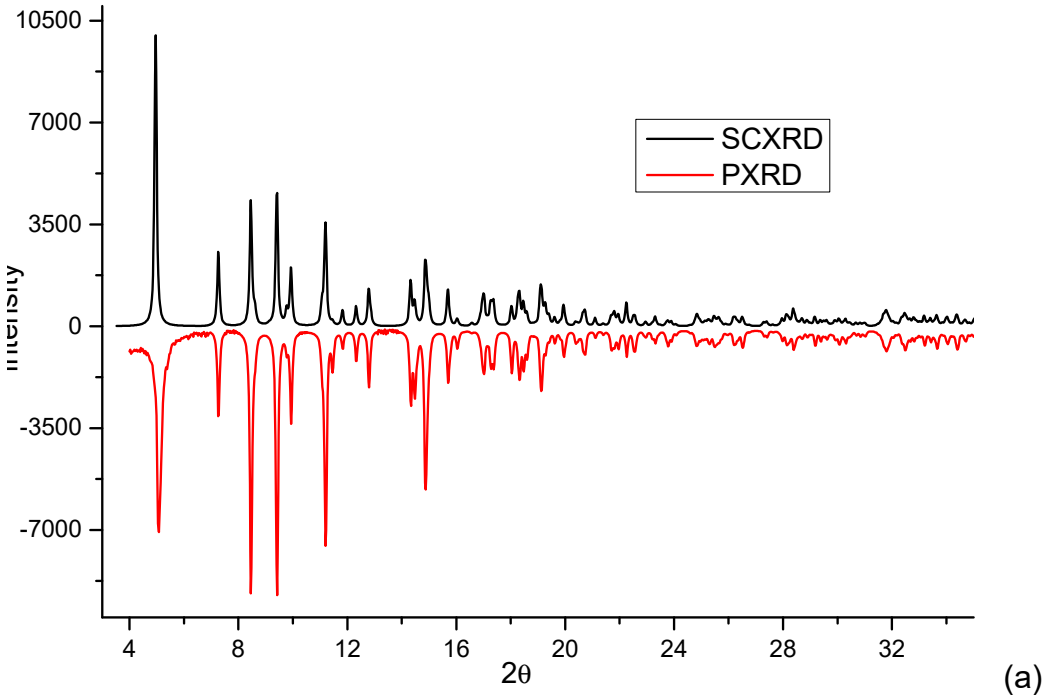

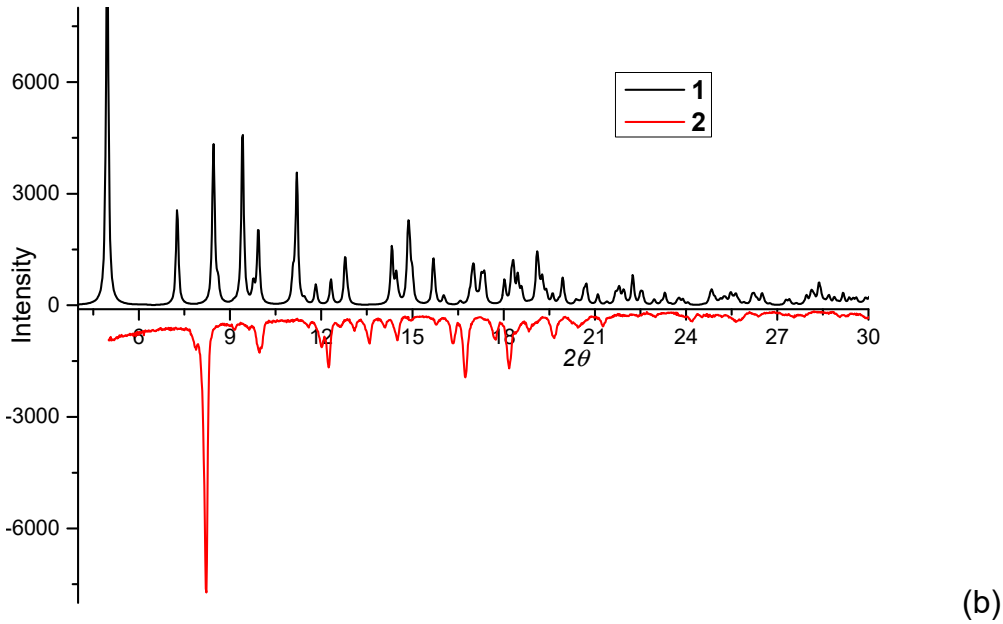

Figure S3. (a) diffractograms for **1**: experimental (red), simulated (black); simulated for **1** (black) and **2** (red).

Preprints (www.preprints.org) | NOT PEER-REVIEWED | Posted: 9 February 2017 doi:10.20944/preprints201702.0029.v1

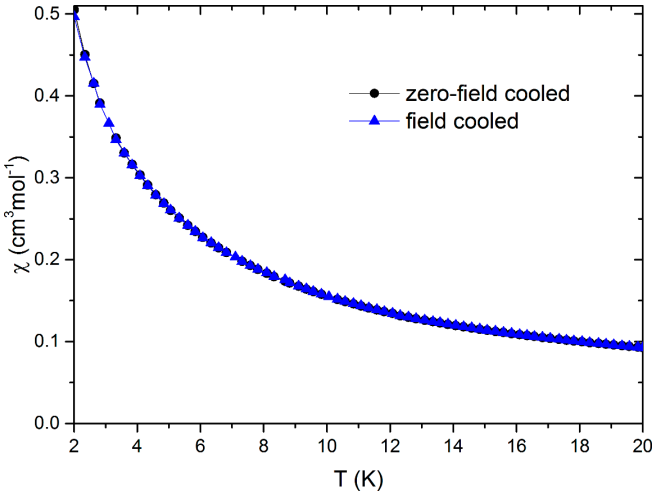

Figure S4 Zero field–cooling/field cooling χ vs ***T*** for **1** (H=20 Oe). Solid lines are to guide the eye.

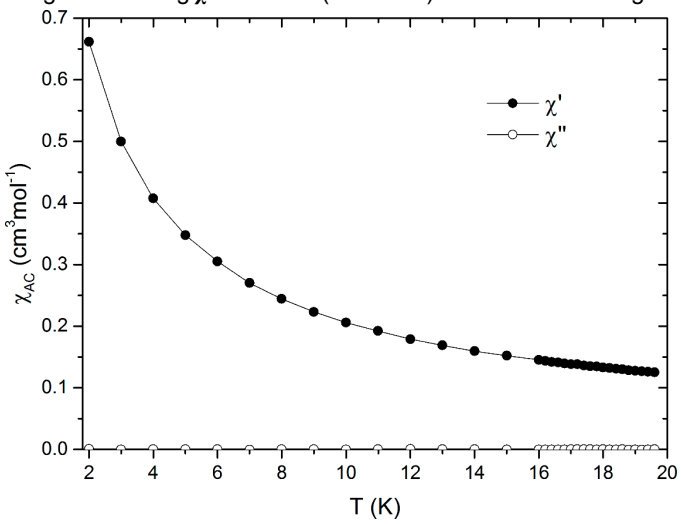

Figure S5. AC susceptibility versus temperature for **1**. H_{AC} = 3 Oe, f_{AC} = 10 Hz. Solid lines are to guide the eye.

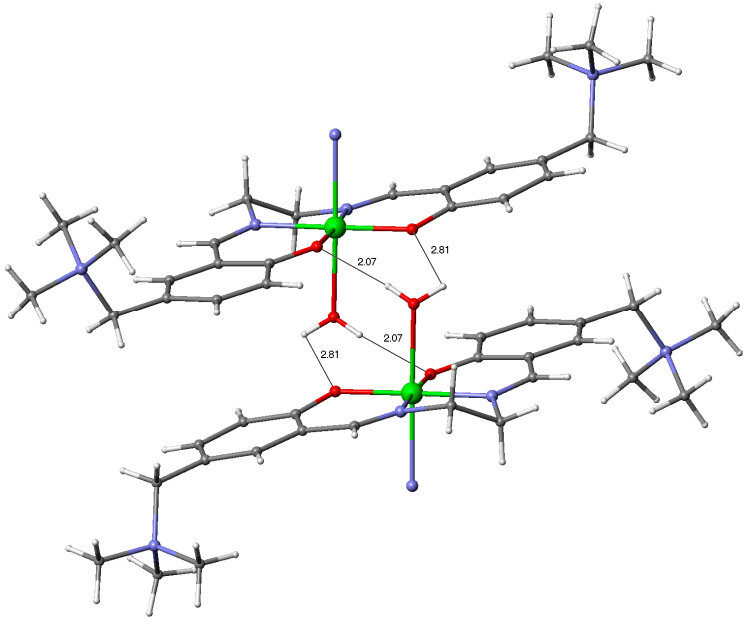

Figure S6. The molecular structure of $[(MnSB^{+}(H_2O)]_2$ dimer in compound I. The O…H hydrogen bonds mediating spin coupling between two Mn^{III} ions (green balls) are shown.

Preprints (www.preprints.org) | NOT PEER-REVIEWED | Posted: 9 February 2017 doi:10.20944/preprints201702.0029.v1

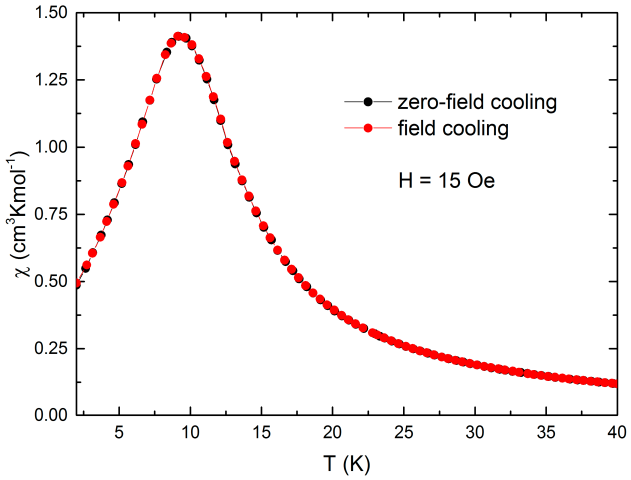

Figure S7. Zero-field cooling and field cooling magnetic susceptibility versus temperature for **2** measured in a DC field of 15 Oe. Solid lines are to guide the eye.

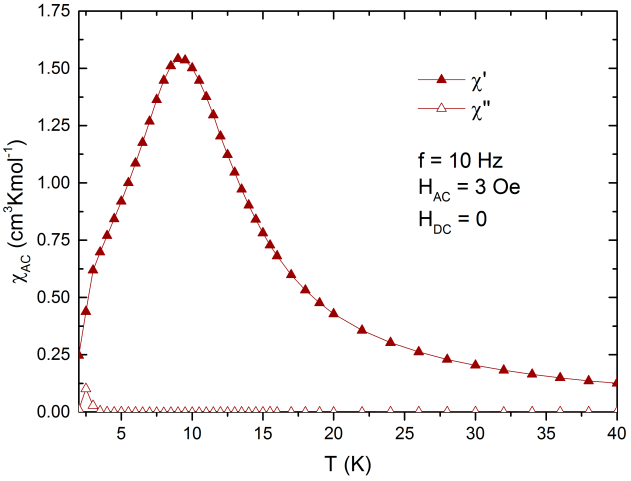

Figure S8. AC susceptibility versus temperature for **2** measured in H_{DC} = 0 Oe and H_{AC} = 3 Oe at f = 10 Hz. Solid lines are to guide the eye.

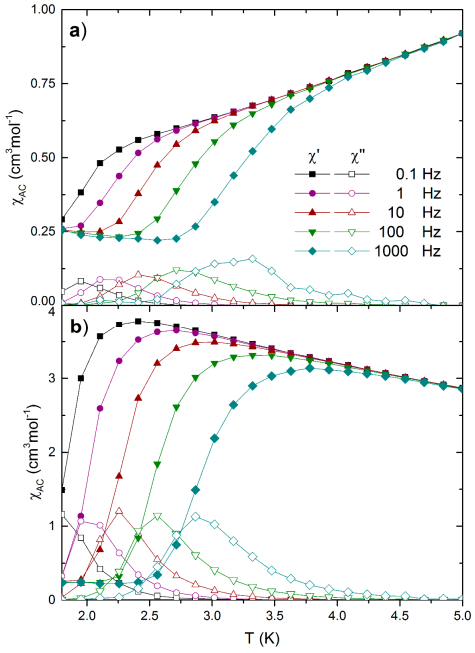

Figure S9. AC susceptibility of **2** as a function of temperature measured over a series of AC frequencies in a) zero DC field and b) DC field of 2 kOe.

Preprints (www.preprints.org) | NOT PEER-REVIEWED | Posted: 9 February 2017 doi:10.20944/preprints201702.0029.v1

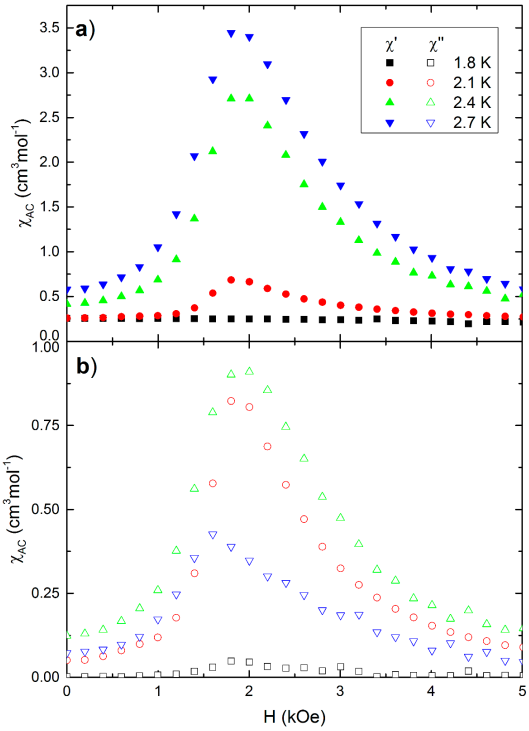

Figure S10. AC susceptibility of **2** as a function of H_{DC} at four temperatures; a) χ', b) χ''. f_{AC}=10 Hz, H_{AC}=3 Oe.

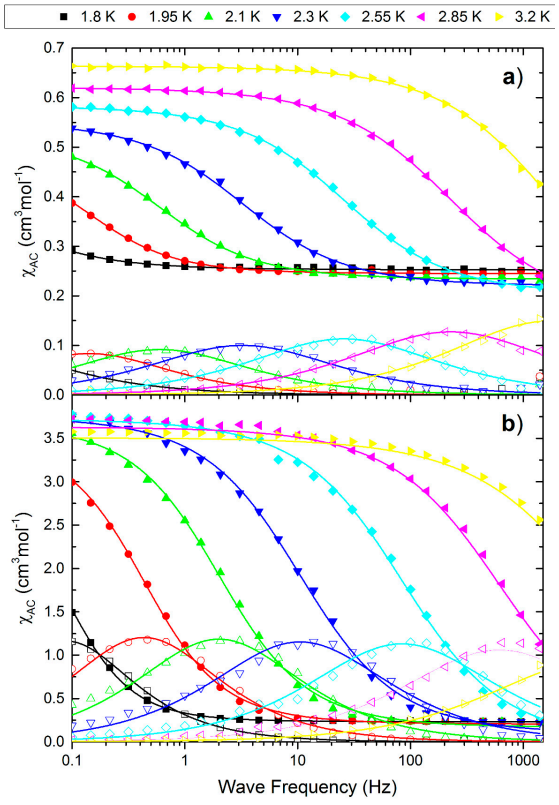

Figure S11. AC susceptibility of **2** measured as a function of AC frequency over a range of temperatures in a) 0 and b) 2 kOe DC field.

Preprints (www.preprints.org) | NOT PEER-REVIEWED | Posted: 9 February 2017 doi:10.20944/preprints201702.0029.v1

Table S1. Parameters τ and α obtained from the generalized Debye model fits to the AC data vs. frequency for sets measured in 0 and 2 kOe DC field.

T (K)	H_{DC} = 0				H_{DC} = 2 kOe			
	τ (s)	Δτ (s)	α	Δα	τ (s)	Δτ (s)	α	Δα
1.8	15	11	0.3	0	1.786	0.044	0.1219	0.0059
1.95	1.13	0.17	0.231	0.035	0.3673	0.0079	0.1968	0.0081
2.1	0.266	0.011	0.283	0.013	0.0794	0.0021	0.244	0.011
2.3	0.04893	0.0016	0.310	0.012	0.01519	$4.5\ 10^{-4}$	0.283	0.012
2.55	0.0062	$1.7\ 10^{-4}$	0.3162	0.0099	0.00190	$4.4\ 10^{-5}$	0.3053	0.0078
2.85	$7.02\ 10^{-4}$	$1.7\ 10^{-5}$	0.3468	0.0062	$2.598\ 10^{-4}$	$4.9\ 10^{-6}$	0.3272	0.0070
3.2	$9.41\ 10^{-5}$	$8.1\ 10^{-6}$	0.341	0.011	$3.612\ 10^{-4}$	$6.8\ 10^{-7}$	0.3753	0.0051